Evolution of ocean circulation in the North Atlantic Ocean during the Miocene: impact of the Greenland ice sheet and the eastern Tethys seaway

Quentin PILLOT[1], Yannick Donnadieu[2], Anta-Clarisse Sarr[3], Jean-Baptiste Ladant[4], and Baptiste Suchéras-Marx[5]

[1]CEREGE
[2]CEREGE (Centre Européen de Recherche et d'Enseignement des Géosciences de l'Environnement)
[3]CEREGE, Aix-Marseille University
[4]Laboratoire des Sciences du Climat et de l'Environnement
[5]Aix-Marseille University, OSU Pythéas

November 22, 2022

Abstract

Modern Ocean is characterized by the formation of deep-water in the North Atlantic (i.e. NADW). This feature has been attributed to the modern geography, in which the Atlantic Ocean is a large basin extending from northern polar latitudes to the Austral Ocean, the latter enabling the connection of the otherwise isolated Atlantic with the Pacific and Indian Oceans. Sedimentary data date the establishment of the NADW between the beginning of the Eocene (49 Ma) and the beginning of the Miocene (23 Ma). The objective of this study is to quantify the impact of Miocene geography on NADW through new simulations performed with the earth system model IPSL-CM5A2. We specifically focus on the closure of the eastern Tethys seaway (dated between 22 and 14 Ma), which allowed the connection between the Atlantic and Indian Oceans, and on the Greenland ice sheet, whose earliest onset remains open to discussion but for which evidence suggest a possible existence as early as the Eocene. Our results show that the closure of the eastern Tethys seaway does not appear to impact the establishment of NADW, because waters from the Indian Ocean do not reach the NADW formation zone when the seaway is open. Conversely, the existence of an ice sheet over Greenland strengthens the formation of NADW owing to topography induced changes in wind patterns over the North Atlantic, which in turn, results in a larger exchange of water fluxes between the Arctic and the North Atlantic, and in a re-localization of deep-water formation areas.

Evolution of ocean circulation in the North Atlantic Ocean during the Miocene: impact of the Greenland ice sheet and the eastern Tethys seaway

Pillot Q.[1], **Donnadieu Y.**[1], **Sarr A-C.**[1], **Ladant J-B.**[2] **and Suchéras-Marx B.**[1]

[1]CEREGE, Aix Marseille Univ, CNRS, IRD, INRAE, Coll. France, France.
[2]Laboratoire des Sciences du Climat et de l'Environnement, LSCE/IPSL, CEA-CNRS-UVSQ, Université Paris-Saclay, France.

Key Points:

- Ocean circulation induced by Early Miocene paleogeography in the IPSL-CM5A2 Earth System model is studied
- No clear impact of the closure of the eastern Tethys seaway is found
- Substantial increase in NADW intensity results from ephemeral Greenland ice-sheets during the Miocene

Corresponding author: Pillot Q., `pillot@cerege.fr`

Abstract

Modern Ocean is characterized by the formation of deep-water in the North Atlantic (i.e. NADW). This feature has been attributed to the modern geography, in which the Atlantic Ocean is a large basin extending from northern polar latitudes to the Austral Ocean, the latter enabling the connection of the otherwise isolated Atlantic with the Pacific and Indian Oceans. Sedimentary data date the establishment of the NADW between the beginning of the Eocene ($\sim$ 49 Ma) and the beginning of the Miocene ($\sim$ 23 Ma). The objective of this study is to quantify the impact of Miocene geography on NADW through new simulations performed with the earth system model IPSL-CM5A2. We specifically focus on the closure of the eastern Tethys seaway (dated between 22 and 14 Ma), which allowed the connection between the Atlantic and Indian Oceans, and on the Greenland ice sheet, whose earliest onset remains open to discussion but for which evidence suggest a possible existence as early as the Eocene. Our results show that the closure of the eastern Tethys seaway does not appear to impact the establishment of NADW, because waters from the Indian Ocean do not reach the NADW formation zone when the seaway is open. Conversely, the existence of an ice sheet over Greenland strengthens the formation of NADW owing to topography induced changes in wind patterns over the North Atlantic, which in turn, results in a larger exchange of water fluxes between the Arctic and the North Atlantic, and in a re-localization of deep-water formation areas.

1 Introduction

One of the drivers of the actual global ocean circulation is the formation of deep water in the North Atlantic Ocean (NADW). At the end of winter, surface waters are denser than the lower layers, because of higher salinity and lower temperature. This initiates a downward convection movement that results in the formation of deep water in this area. This movement causes an export of cold and dense water to the Southern Ocean while a compensatory flow of intermediate water rises to the north, the Antarctic Intermediate Water (AAIW), that close the circulation cell. When North Atlantic deep waters leave the northern subpolar regions (between 2000 m and 4000 m depth), they cross the equator and enter the southern hemisphere, then a part are dragged into the Antarctic Circumpolar Current (ACC) and redistributed into the Pacific, Atlantic and Indian basins whereas another part upwelled in the Southern Ocean (Talley, 2013). The association with the AABW (Antarctic Bottom Water) forms the Atlantic Meridional Overturning Circulation (AMOC). The two layers structure of the modern AMOC arise from the particular state of the Atlantic basin geometry with a closed Central American seaway and open Drake passage (Ferreira et al., 2018). During Cenozoic times and, in particular, the Miocene period, the physical structure of the AMOC was probably different because the configuration of major gateways and submarine topographic barriers in the Atlantic and Pacific basins differ substantially. From the Miocene to today, these changes include the deepening of the Greenland-Scotland Ridge (GSR), opening of the Fram Strait (FS) and closing of the Bering Strait (BS) in the northern latitudes; the closure of the Central American Seaway (CAS) and Eastern Tethys Seaway (ETS) in tropical latitudes; and the potential narrowing of the Drake Passage (DP) in the southern latitudes. Apart those change in the seaways and the Eurasiatic land-sea mask, the continents configuration during the Miocene period was close to the modern one with some substantial changes in the topography worldwide (Poblete et al., 2021).

Several studies have been dedicated to the geological history of the deep water formation in the North Atlantic over the Cenozoic, both using Earth system models of various complexities and paleoceanographic data. Among those data, researchers have relied on sedimentary drift deposits, on Nd isotopes and on oxygen and carbon isotopes.Many studies suggest the onset of NADW formation during the Eocene (Borrelli et al., 2014; Langton et al., 2016; Coxall et al., 2018; Via & Thomas, 2006; Wright & Miller, 1993; Davies et al., 2001) sometimes called NCW (North Component Water) which refers to an early version of the NADW. The NCW was not part of a large and extensive overturning cell as the present NADW. Borrelli et al. (2014) reported similar benthic foraminifera $\delta^{18}O$ and $\delta^{13}C$ signatures at site ODP1053 (upper deep water, western North Atlantic) and at sites located in the Southern Ocean, equatorial Pacific, and western Atlantic until the end of the middle Eocene (39-40 Ma). Around 38.5 Ma, the values between North Atlantic, Southern and Pacific oceans began to differentiate leading Borrelli et al. (2014) to suggest an onset of NCW due to a gradual opening of the Southern Ocean gateways. Langton et al. (2016) used the same methodology on sites further south in the Atlantic Ocean (30°S) and find a close date for the initiation of NCW (38 Ma). However, the GSR was too shallow at 38 Ma to allow waters to reach the subarctic seas and cool enough to dive, thus other studies propose that tectonic adjustments of the GSR would have initiated the NCW between 36 Ma (Coxall et al., 2018) and 34-33 Ma (Via & Thomas, 2006; Wright & Miller, 1993). Independent evidence from sedimentary deposits in the Faroe Shetland Basin indicate that NCW may have begun around 35 Ma Davies et al. (2001). Later, the transition from NCW to NADW may have been initiated by the intensification of the ACC at a time of a deepening of the Drake Passage in the late Oligocene (Katz et al., 2011). Moreover, Scher and Martin (2008) correlated the widening of the Drake Passage with the intensification of NCW/NADW because the long-term decreasing trend in neodymium isotopes values on the Agulhas Ridge (Atlantic sector of the Southern Ocean) suggests that the export of NCW/NADW from the North Atlantic to the Southern Ocean increased during the Oligocene and Miocene. In more recent geological time, different seaways influenced NADW dynamics. Cenozoic sediment cores from the Arctic's deep-sea floor revealed more ventilated waters in the Arctic Basin related to enhanced NADW about 17.5 Ma ago due to the opening of the Fram Strait and increased exchanges between North Atlantic and Artic oceans (Jakobsson et al., 2007). Woodruff and Savin (1989) used isotopic data from benthic foraminifera to suggest that the closure of the eastern Tethys seaway connecting the Indian Ocean to the Mediterranean Sea caused saltwater to enter the North Atlantic, intensifying NADW around 14.5 Ma. Short-term fluctuations in NADW after 12 Ma are controlled by vertical movements of the GSR (Poore et al., 2006) based on the study of $\delta^{13}C$ gradients in benthic foraminifera from several oceans (Atlantic, Pacific, and Southern).

From a modeling point of view, earlier studies such as the one of von der Heydt and Dijkstra (2006) found a meridional overturning circulation substantially different than the present-day circulation and characterized by a weaker and shallower NADW with the presence of deep-water formation in the North Pacific, using both Oligocene and Miocene paleogeographies. This pattern is rather accepted in the community and thus recent studies have focused on the role of marine gateways from both equatorial and high latitudes (Z. Zhang et al., 2011). Specifically, modeling studies suggest that the closure of the CAS enabled an intensification of NADW (Sepulchre et al., 2014; Schneider & Schmittner, 2006; Nisancioglu et al., 2003). Coupled ocean/atmosphere simulations also indicate greater NADW when the GSR is deeper (Stärz et al., 2017; Hossain et al., 2020). The opening of the Bering Strait however decreased NADW although this effect is offset by the closure of the CAS, according to modeling studies by Brierley and Fedorov (2016) and Hu et al. (2015). Compared to other major seaways such as the CAS or Drake Passage, the eastern Tethys seaway has only drawn limited attention (Hamon et al., 2013) and no updated study has tested the role of this seaway on the emergence and strength of the NADW using an up-to-date early Miocene paleogeography. Finally, conversely to paleogeography as mentioned above, the effect of an ice-sheet on Greenland on the generation of the NADW in an early Miocene world has never been tested despite evidence of glaciation in this region dating back to the Oligocene (Bernard et al., 2016) and the known impact of this ice-sheet in the formation of the NADW (Davini et al., 2015).

In the present study, we aim to discuss the dynamics of the NCW/NADW considering the rather unexplored influence of an open eastern Tethys seaway and of an ice-sheet over Greenland. We simulate the ocean dynamics using the IPSL-CM5A2 with a fixed pCO_2 and updated paleogeography of the Early Miocene proposed by Poblete et al. (2021), which exhibits open connections between the Pacific, Atlantic and Artic oceanic basins through the Central America Strait, the Fram Strait, the Greenland-Scotland Ridge and the Drake Passage.

2 Method

2.1 Model

The Earth System Model used in this study is IPSL-CM5A2 (Sepulchre et al., 2020) that is an updated version of IPSL-CM5A-LR model (Dufresne et al., 2013), with bias corrections and reduced computational times to perform multimillennial simulations typical of paleoclimate studies. It is composed of the NEMO ocean model (Madec, 2015) which includes the PISCES-v2 model for biogeochemistry (Aumont et al., 2015), the OPA8.2 model for ocean dynamics (Madec, 2015) and the LIM2 model for sea ice (Fichefet & Maqueda, 1997). IPSL-CM5A2 is also composed of the atmospheric model LMDZ (Hourdin et al., 2013) and the land surface and vegetation model ORCHIDEE (Krinner et al., 2005). The OASIS coupler (Valcke, 2013) connects the atmospheric grids (96x96 or 3.75° in longitude and 1.875° in latitude over 39 vertical levels) and oceanic grids (resolution of about 2° that decreases to 0.5° in the tropical region over 31 vertical levels, whose thickness varies from 10 m near the surface to 500 m near the bottom of the ocean). More details about model parameterization can be found in Sepulchre et al. (2020).

2.2 Experiments and boundary conditions

2.2.1 Control simulation

Three simulations were run in this study with a paleogeography corresponding to the early Miocene (20 Ma) from the study of Poblete et al. (2021) (Figure S1). In this paleogeography, most of the mountain belts are lower than today, there is a modern Antarctic ice-sheet and the Paratethys shallow sea covers part of Central and Eastern Europe with a connection to the Mediterranean Sea. The CAS is open but shallow, the Bering Strait is closed, the Fram Strait is narrower than today, and the GSR is deep (Figure S2). In absence of worldwide reconstruction for paleo-vegetation in the early Miocene, we used idealized vegetation with a latitudinal distribution. The atmospheric pCO_2 level for the three simulations is set to 560 ppm (Sosdian et al., 2018; Rae et al., 2021) and other parameters such as the other greenhouse gases and orbital parameters are set to their pre-industrial values. The first simulation (MioCTL, Table 1) is used as a reference for sensitivity tests. In this simulation there is no ice sheet on Greenland and the eastern Tethys seaway is closed. This simulation have been used in the simulation compilation of Burls et al. (2021) and show the same classical features than others models when compared to data with a good fit at low to mid-latitudes and a poorer fit to the global warmth inferred from data at higher latitudes. Mainly, simulating the low meridional temperature gradient reconstructed from Miocene data remains an outstanding problem for most models.

2.2.2 Simulation with a Greenland Ice Sheet (GIS)

The second simulation, MioGIS, is identical to the first one but Greenland is covered by a modern-size ice sheet in order to maximize the potential of its direct effects—the larger elevation and the higher albedo compared to the no ice sheet case—on NADW. The date of onset of Greenland ice sheet indeed remains debated. It is often considered that the GIS appears in the Pliocene (Butt et al., 2001; Knutz et al., 2015), based on sedimentological analyses from the East Greenland margin, and marine seismic reflection (contourites) from the West Greenland margin. However, Eldrett et al. (2007) and Tripati et al. (2008) infer evidence of Eocene and Oligocene (48-30 Ma) glaciation in the form of IRD (Ice-Rafted Detritus) in the Norwegian Sea. Bernard et al. (2016) demonstrate the presence of erosion on the eastern coast of Greenland around 30 Ma using thermochronological dating. This set of evidence indicates possible glaciation events (partial or total) over Greenland since the early Eocene. Studies have also demonstrated glaciations during the late Miocene (11 Ma and 7 Ma) through the presence of IRD and dropstones in Irminger Basin sediments (Helland & Holmes, 1997; John & Krissek, 2002; Bierman et al., 2016). Finally, using an isotope-capable global climate/ice-sheet model, DeConto et al. (2008) indicate that episodic glaciations in the Northern Hemisphere are possible since 25 Ma.

2.2.3 Simulation with an open eastern Tethys seaway

The third simulation, MioTet120, is identical to the control simulation, but the eastern Tethys seaway is open with a depth of 120 meters and a width of 390 km at its narrowest section. This depth was chosen to allow a significant surface flow exchange between the Mediterranean Sea and the Indian Ocean while agreeing with the configuration of a restricted pre-closure state. As with the onset of the GIS, the tectonic history and closure chronology of the eastern Tethys seaway is debated (Allen & Armstrong, 2008). They suggest a closure age during the late Eocene (approximately 35 Ma), based on the study of deformation and uplift during the collision between the two tectonic plates. Hüsing et al. (2009) suggest a more recent age for the closure of the eastern Tethys seaway (28 Ma) based on biostratigraphic studies in the north of the Bitlis-Zagros suture zone. However, many paleogeographic and paleontological studies indicate an early Miocene closure (Rögl, 1999; Reuter et al., 2009; Harzhauser et al., 2009). Bialik et al. (2019) use neodymium isotope records from both sides of the seaway and suggest that water mass exchange between the Mediterranean and Indian Ocean was reduced by 90% around 20 Ma. This age is also proposed by Okay et al. (2010) using apatite fission track ages from the Bitlis-Zagros thrust zone. Biostratigraphical and paleontological data indicate that the Mediterranean Basin and Indian Ocean were intermittently connected until at least the middle Miocene (Rögl, 1999; Harzhauser et al., 2007, 2009; Sun et al., 2021). Through magnetostratigraphic and biostratigraphic studies on sediments from the Zagros Basin, (Sun et al., 2021) indicate that the eastern Tethys seaway changed from a partially open seaway to a restricted connection and then to an intermittently open seaway. They suggest that marine transgressions and regressions controlled by astronomical factors (100 ka cycles) have caused these reopening phases. The final closure is generally dated to the middle and late Miocene between 14 and 11 Ma (Bialik et al., 2019; Sun et al., 2021; Rögl, 1999; Hüsing et al., 2009) and may probably be caused by a significant drop in sea level driven by the growth of the ice sheet over Antarctica (Sun et al., 2021; Bialik et al., 2019).

Table 1. Experimental Design

Simulation	Geography	pCO_2	Eastern Tethys seaway	GIS	Simulation length
MioCTL	20Ma	560ppm	closed	no	3000 year
MioGIS	20Ma	560ppm	closed	yes	3000 year
MioTet120	20Ma	560ppm	open (120m)	no	3000 year

3 Results and discussion

In the following we first describe the impact of Miocene paleogeography on AMOC and then discuss the respective influence of GIS and eastern Tethys seaway.

3.1 Impacts of Miocene paleogeography

Our MioCTL simulation exhibits spatial patterns of temperature and salinity relatively similar to the preindustrial simulation (this simulation called PREIND is taken from Sepulchre et al. (2020)) with warm and salty waters extending northward across mid-latitudes in the eastern part of the North Atlantic basin while fresher and cooler waters spread over the western part covering the entire Labrador Sea (Figure 1 a). The freshest conditions in the North Atlantic basin are found all along the eastern coast of Greenland and originated from the Arctic Basin across the narrow and shallow early Miocene Fram strait used in our paleogeography (Figure S2).

Deep water formation occurs in the North Atlantic Ocean over an area located between 20 and 30°W and between 55 and 60°N, as inferred by a deep winter mixed layer reaching locally 1000 m. Comparison with modern features simulated in IPSL-CM5A2 (Figure 1) shows that the spatial extent of the sinking zone in the North Atlantic is reduced as well as the strength and vertical extension of the meridional overturning circulation (Figure 1 b and 2). In the MioCTL simulation, the AMOC reaches 1700 m in depth and extends to 60°S (Figure 2) with a maximum intensity of 5 Sv in the North Atlantic Ocean (at 37°N and 1000 m) whereas the simulated preindustrial AMOC is 11 Sv and extends down to 3000 m. This is in agreement with previous studies showing the major impact of the opened CAS (Sepulchre et al., 2014; Schneider & Schmittner, 2006; Nisancioglu et al., 2003) on the intensity of NADW formation. We also note that our Miocene simulations were performed without tidal forcing in absence of an available reconstruction, which may induce a weaker overturning in the deepest layers of the ocean and explain the less intense Antarctic Bottom water formation despite a deeper mixed layer depth found in our Miocene simulations (Y. Zhang et al., 2020). No deep-water formation occurs in the North Pacific in any of our simulations. In the South hemisphere, deep-water areas are located both in the Atlantic and the Indian part of the Austral Ocean and sinking waters reach greater depth (1000 to 2500 m) than in the North Atlantic (Figure S3).

Because we have imposed a doubling of the atmospheric pCO_2, SSTs are warmer during the Miocene than at present-day with heterogeneous spatial patterns. Two areas of warming well above the average are located first eastward of North America between 30 and 40°N and second in the Greenland-Iceland-Norwegian Seas with SST differences exceeding 5°C compared to PREIND (Figure 1 b). Surface salinity is lower during the Miocene owing to the increased hydrological cycle occurring in a warmer climate at latitudes where the precipitation minus evaporation budget is found to be positive (subtropics, Herold et al. (2011),Burls and Fedorov (2017)). In contrast, subtropical salinities are larger during the Miocene owing to a more negative P-E budget occurring at these latitudes (not shown). Finally, the positive salinity anomaly located southward of Greenland matches the only area where mixed layer depth is deeper in our MioCTL simulation compared to the PREIND simulation.

Herold et al. (2011) also observe a less intense NADW in their Miocene simulation compared to their modern simulation. In their Miocene simulation, the mixing layer depth (150 metres) is much shallower than in MioCTL but the NADW cell depth (1500 metres) is similar to MioCTL. The shallower deep water formation in the Miocene compared to the present day is explained by less salty waters in the North Atlantic. However, they observe colder surface water temperatures in the Miocene than in the present. This is not in agreement with our results and is explained by the pCO_2 level in their simulations which is maintained at the same level in the Miocene as in their modern reference (355 ppm).Krapp and Jungclaus (2011) find no significant difference in the intensity of NADW and AMOC between their Miocene simulation and their modern simulation. This difference to our results can be explained by their low pCO_2 level at 360 ppm because in another of their simulations with pCO_2 at 720 ppm, there is almost no NADW. This difference is also due to the salinity of surface waters in the North Atlantic which is equivalent in the Miocene and in the present (not the case in our study). They attribute this to the inflow of salt water from the Mediterranean (open eastern Tethys seaway) which compensates for the cooling by the CAS. The salinity input from the Mediterranean when the eastern Tethys seaway is open will be discussed below.

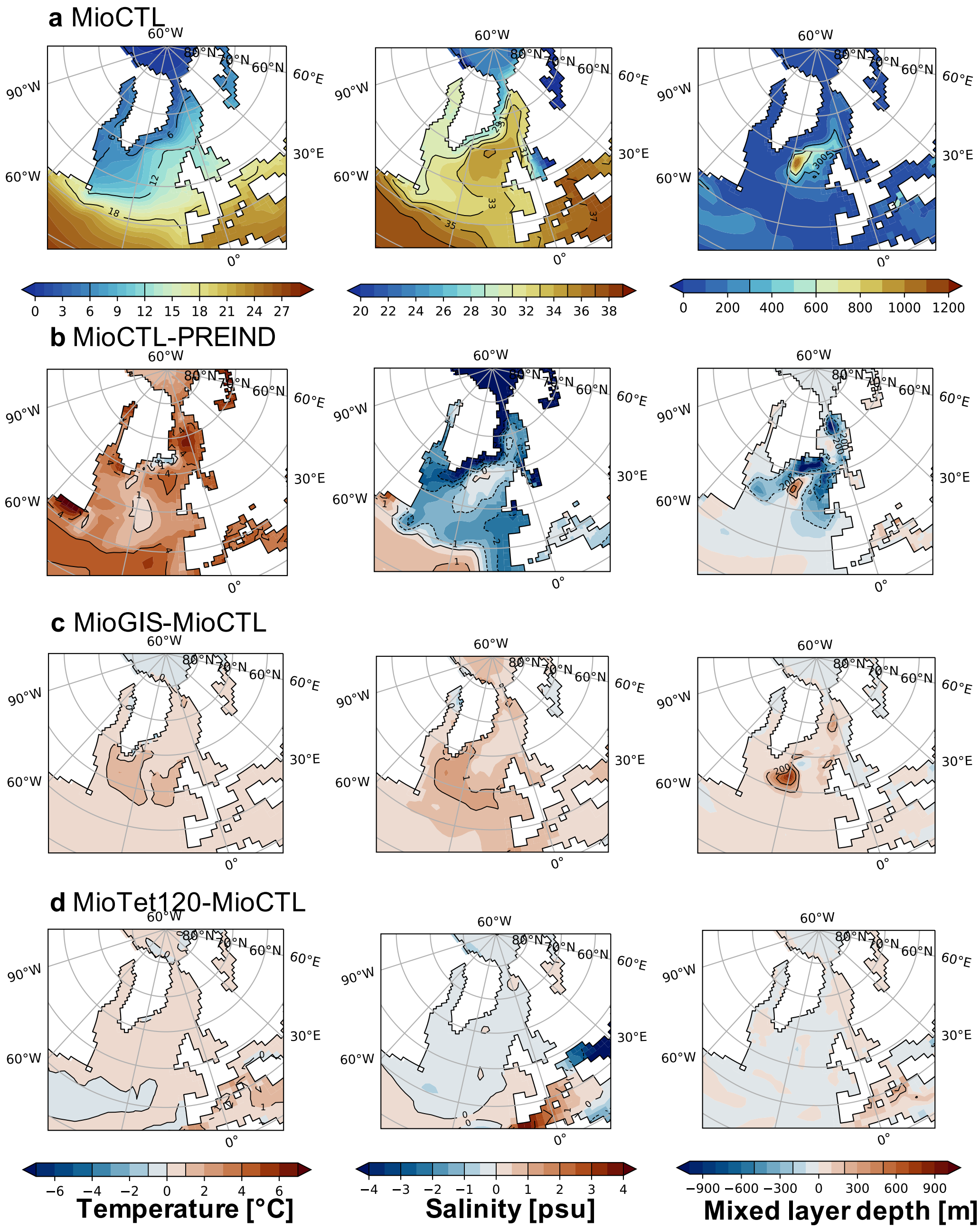

Figure 1. Left column, SST (°C) averaged over the year. Middle column, SSS (psu) averaged over the year. Right column, mixed layer depth (mld, metre) averaged over the winter (January-February-March). (a) MioCTL simulation. (b) Difference between the MioCTL control simulation and the pre-industrial simulation (PREIND). (c) Difference between the MioGIS simulation and the MioCTL simulation. (d) Difference between the MioTet120 simulation and the MioCTL simulation.

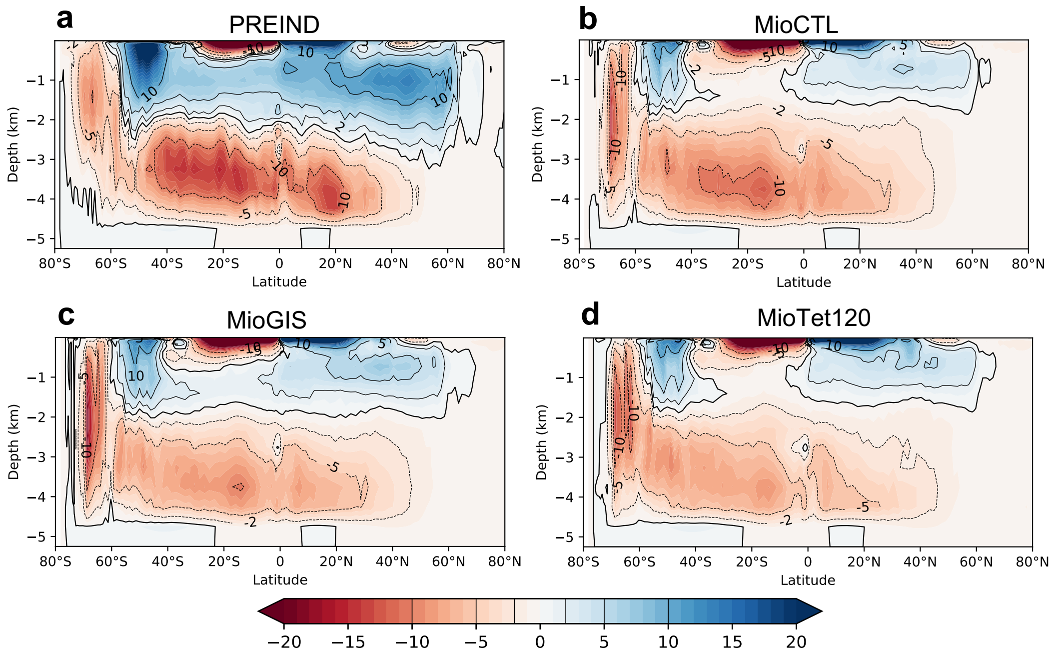

Figure 2. Meridional Overturning Circulation (MOC) computed from the global ocean. (a) PREIND (b) MioCTL (c) MioGIS and (d) MioTet120. In blue, the water masses rotate clockwise and in red, counterclockwise. Unit: Sv; horizontal axis: latitude in degrees; vertical axis: depth in kilometers.

3.2 Ocean Atmosphere feedback induced by the Greenland ice-sheet

With a Greenland ice-sheet during the Miocene, the AMOC strengthens by 33% from 6 Sv to 8 Sv (Figure 2 and S4) and the North Atlantic becomes saltier from 0.5 to 1.5 psu. The formation zone of the NADW extends westward and covers the region 15° to 40°W and 50° to 60°N, and waters sink deeper down to 1500 m (Figure 2 c). In this simulation, there is another area of deep-water formation in the Greenland Sea (0°E, 70°N) where the depth of the mixed layer reaches 500 m. The salinity difference between the two simulations (MioCTL and MioGIS) may come from the exchange between the Arctic Basin and the North Atlantic ocean. The freshwater input from runoff into the Arctic basin is the same in both simulations. However, the precipitation minus evaporation (P-E) balance in this basin is slightly higher in the presence of the GIS (+7 mSv, Figure 3 and S5 c). In the North Atlantic basin, the P-E is similar in both simulations but the runoff is slightly higher in MioCTL (+8 mSv). Overall, the GIS causes a larger freshwater input in the North Atlantic/Arctic oceans. This is in contradiction with the fact that the waters are saltier in the North Atlantic and the Arctic Basin in the MioGIS simulation. To explain this salinity anomaly, it is necessary to look at the ocean dynamics in response to the modification of the topography over Greenland owing to the presence of the ice-sheet.

In the MioCTL simulation, there is an atmospheric low pressure cell east of Greenland that extends over land (Figure S5 a). The center of this low pressure cell is located at latitude 67°N in the Norwegian Sea. This cell generates surface winds that facilitate the exchange of water between the North Atlantic and the Norwegian Sea via the wind-driven surface circulation. The presence of the ice-sheet topography in MioGIS compared to MioCTL prevents this cell from advancing inland and its center is consequently further south than in MioCTL (57°N). Indeed, in MioGIS, a stable high-pressure area is present over Greenland, causing strong winds along the eastern coast of the landmass (consistent with the results of Lunt et al. (2004) and Toniazzo et al. (2004)). The katabatic winds coming down from the reliefs are caught in this low-pressure area and reinforce it. The wind stress over the Norwegian Sea is higher in the MioGIS simulation (Figure S5 b).

These southward winds force the surface currents to move southward as well. This increases water exchange between the Arctic and the North Atlantic basins in MioGIS in comparison to MioCTL. Exchanges between the North Atlantic and the Arctic basins are limited by the geography of the Miocene in which the only connection is the Fram Strait, which is much narrower than today. Through the Fram Strait, a deep current between 350 and 700 m depth brings waters from the North Atlantic to the Arctic. These waters circulate and upwell in the Beaufort anticyclonic gyre where they are cooled. A surface current between 0 and 350 m depth leaves the Arctic Basin and reaches the North Atlantic along the east coast of Greenland. In the MioGIS simulation, there are 1.412 Sv of water flowing into the Arctic basin and 1.690 Sv flowing out of it. In the MioCTL simulation, these numbers are respectively 1.265 Sv and 1.537 Sv (Figure 3). The balance of incoming minus outgoing water in both simulations is negative because there is an input of fresh water in the Arctic Ocean from the atmosphere (P-E and runoff). The salt concentration of outgoing waters is therefore lower than incoming waters. Numerically, the GIS causes a 147 mSv increase in water flow from the North Atlantic to the Arctic and a 153 mSv increase in water flow from the Arctic to the North Atlantic. This explains why the Arctic Basin waters are saltier in the MioGIS simulation. In pre-industrial conditions, water input from the Arctic Basin slows down the NADW because the lower salinity of these waters compared to those of the North Atlantic increase the buoyancy of the surface waters in the North Atlantic. This slowdown is attenuated in the presence of GIS because the waters from the Arctic Basin are saltier (+1 psu).

With a Greenland ice-sheet during the Miocene, the sea surface temperature in the North Atlantic is higher (+1°C), which leads to a decrease in sea-ice formation in coastal Greenland and in the Labrador Sea in MioGIS compared to MioCTL (Figure S6). These results show that the cooling effect of the ice sheet does not extend beyond Greenland because it is hampered by other dynamical processes, such as a geopotential anomaly due to the appearance of orographically induced Rossby stationary waves (Maffre et al., 2018) or the increase in deep water formation driving heat input to the North Atlantic via the temperature-advection feedback.

Our results are consistent with those of Davini et al. (2015), who observe a slowdown of AMOC by 12% in the absence of an ice sheet over Greenland (25% in our case) in a modern configuration. Though their simulated slowdown is weaker, probably because of a combination of a different model, pCO_2 levels and geography—and, in particular, the configuration of the Fram Strait (Hossain et al., 2020)—, it is interesting to note that they also attribute the slowdown signal to the exchanges between the Arctic and the North Atlantic basins.

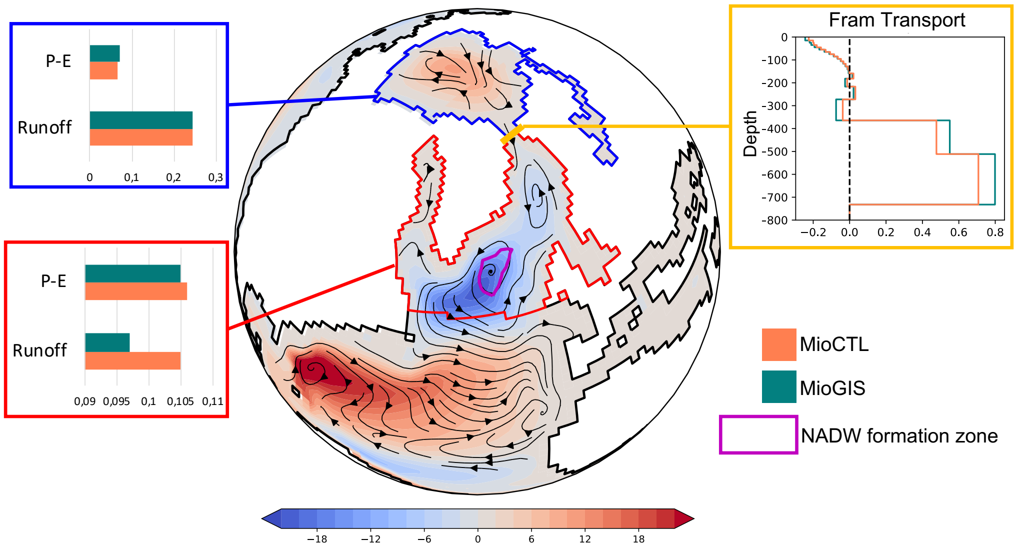

Figure 3. The map shows the mean annual barotropic stream function, in Sv, for the MioCTL simulation (in blue, the water masses rotate counterclockwise and in red, clockwise). The blue box shows the precipitation-evaporation (P-E) balance and runoff (in Sv) for the Arctic basin. The red box shows the precipitation-evaporation balance (P-E) and the runoff (in Sv) for the North Atlantic Basin. The yellow box shows the water mass exchanges at the Fram strait (in Sv), positive towards the north and negative towards the south.

3.3 Consequences of the closure of the eastern Tethys seaway on water exchanges between the Indian and Atlantic Oceans and the Mediterranean Sea

Opening the eastern Tethys seaway at 120 m depth, on the other hand, results in negligible changes in terms of SST, surface salinity and mixed layer depth (Figure 1 d) in the North Atlantic and Arctic Oceans. The AMOC index is also relatively similar to the one of MioCTL (Figure S4). We explain below the reasons why the AMOC appears insensitive to changes in Tethys seaway, contrasting to previous modeling results (Z. Zhang et al., 2011) and commonly-accepted hypothesis in the literature (Woodruff & Savin, 1989; Wright et al., 1992).

First, the closure of the eastern Tethys seaway causes a restructuring of water exchanges between the Mediterranean Sea and the Atlantic and Indian Oceans. In MioCTL, water exchange is only possible between the Mediterranean Sea and the Atlantic Oceans through the Gibraltar gateway. Surface water flow is directed from the Atlantic Ocean to the Mediterranean Sea whereas subsurface flow is reversed (Figure S7 and 8). The difference between water flowing in and out of the Mediterranean Sea is smaller than 100 mSv (2.18 Sv in and 2.09 Sv out, compensated by runoff and P-E). In MioTet120, the majority of the water entering the Mediterranean basin comes from the Indian Ocean (3.8 Sv) and then flows into the Atlantic Ocean (4.06 Sv). This net westward flow through the Mediterranean sea is a remnant of the circumglobal Tethys current (de la Vara & Meijer, 2016). Most modeling studies (von der Heydt & Dijkstra, 2006; Herold et al., 2011; Karami, 2011) describe an overall net flow in the eastern Tethys seaway that is directed toward the Mediterranean Basin, with water transported from the Indian to the Atlantic through the Mediterranean Sea as seen in our simulations. In our simulations, there also exists a water flux that flows at depth from the Atlantic Ocean to the Mediterranean sea which is consistent with the results of Karami (2011).

Outflowing waters from the Mediterranean Sea are dragged into the North Atlantic Gyre along the North African coasts and then cross the Atlantic Ocean into the Caribbean Sea. Consequently, waters originating from the Indian Ocean return to the low latitudes in the Atlantic Ocean and hardly influence North Atlantic Ocean conditions, which explains the small difference between MioTet120 and MioCTL in the area of deep water formation in the North Atlantic. In addition, we note that there is almost no salinity gradient at the latitudes of the eastern Tethys seaway between the Indian and the Atlantic Oceans, at least for shallow depths (Figure 4 b), suggesting that there is no significant salt transport between these two oceans. The closure of the eastern Tethys seaway also impacts water flow exchange between the Atlantic and Pacific Oceans across the CAS. In MioCTL, 6.21 Sv of waters is transported from the Atlantic to the Pacific and 13.84 Sv from the Pacific to the Atlantic. In MioTet120, more water is transported to the Pacific (+1.33 Sv) and less to the Atlantic (-2.51 Sv). This indicates that the extra water entering the Atlantic from the Mediterranean when the eastern Tethys seaway is open is mainly discharged to the Pacific through the CAS (consistent with Herold et al. (2011)).

Many studies suggest that the eastern Tethys seaway was shallow or even intermittent as early as 22 Ma (Rögl, 1999; Harzhauser et al., 2007, 2009; Sun et al., 2021; Bialik et al., 2019). Our results are consistent with those of Hamon et al. (2013) in suggesting that the final closure of the eastern Tethys seaway in the Miocene did not generate major changes in the Atlantic meridional circulation, although the details of our and Hamon et al. (2013) simulations differ, in particular the depth of the eastern Tethys seaway and Gibraltar gateway. As such, even though the eastern Tethys seaway is shallower in our simulation than in Hamon et al. (2013), the flux through Gibraltar towards the Atlantic Ocean is higher (4 Sv versus 2.8 Sv in Hamon et al. (2013)) because the Gibraltar gateway is deeper in our paleogeography (1350 m versus 400 m in Hamon et al. (2013)). Hence, the influence of the Mediterranean seaways on the Atlantic circulation in the Miocene may be related to the dynamics of Gibraltar gateway (Ng et al., 2021; Capella et al., 2019; Flecker et al., 2015; Ivanovic et al., 2013).

In the modeling study by Z. Zhang et al. (2011), the simultaneous closure of the CAS and the Tethys Seaway causes an amplification of NADW, which is not the case in our study. However, it is difficult to know whether it is the closure of the CAS or the Tethys Seaway that causes this amplification. We note however that a significant number of studies have shown that a primary effect of closing the CAS is to amplify NADW (Sepulchre et al., 2014; Schneider & Schmittner, 2006; Nisancioglu et al., 2003) and we speculate that it is probably the key driver of NADW increase in the results of Z. Zhang et al. (2011). In addition, Z. Zhang et al. (2011) use an Early Eocene paleogeography that is quite different from the Early Miocene and thus could also partly explain the contradictory results with our simulations.

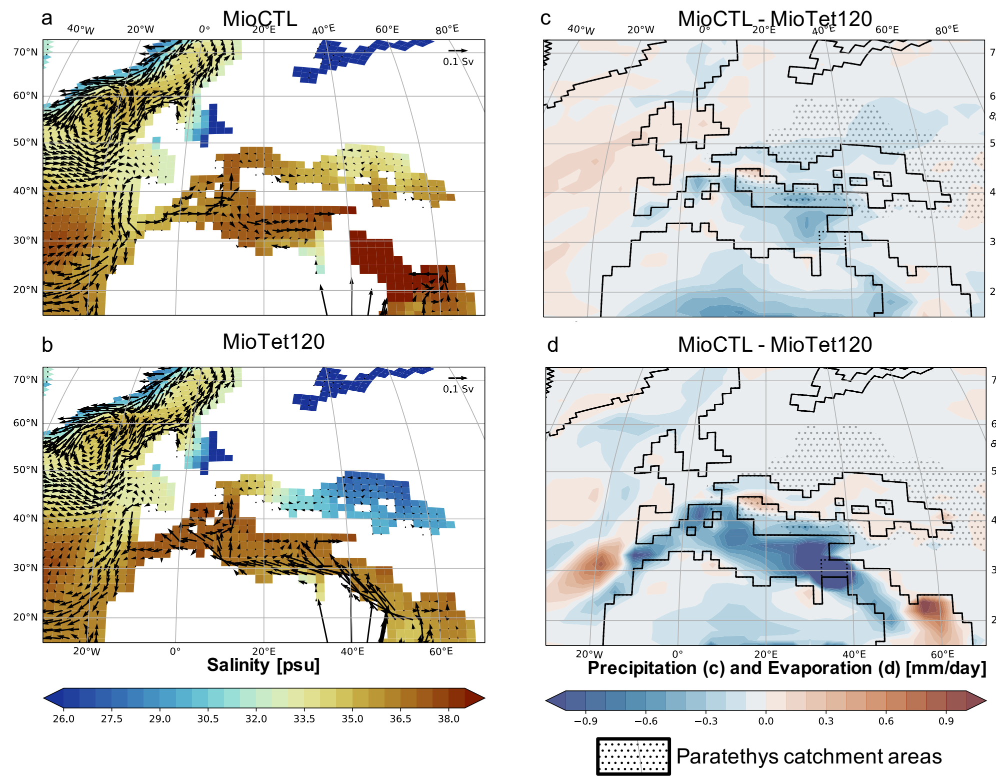

Figure 4. Left: Salinity (psu) for the first 100 meters averaged over the year. The arrows indicate the direction of the flows and the streamflow in Sv (averaged over the year) (a: MioCTL and b: MioTet120). Right, c : Differences in precipitation in mm/day averaged over the year (MioCTL-MioTet120). Right, d: Differences in evaporation in mm/day averaged over the year (MioCTL-MioTet120). The dotted areas represent the catchment's areas draining into the Paratethys.

Although the closure of the eastern Tethys seaway has no impact on surface salinity of the North Atlantic, there is a significant salinity anomaly in Paratethyan waters (Figure 1 c). In MioTet120, the Paratethys is considerably less salty than in MioCTL (-5 psu). When the eastern Tethys seaway is closed, the salinity is relatively homogeneous between the Mediterranean sea and the Paratethys (Figure 4 a and b). There is a 6 mSv freshwater inflow (precipitation - evaporation + runoff) in the Paratethys in the MioTet120 simulation whereas it is restricted to -1 mSv in the MioCTL simulation. This difference in freshwater inflow is explained by higher precipitations over the Paratethys and its catchments (Figure 4 c) with the eastern Tethys seaway open. This additional water inflow in the MioTet120 simulation comes from a more humid atmosphere. By closing the eastern Tethys seaway, a water surface is removed and replaced by a land surface causing a large negative evaporation anomaly at the seaway location (Figure 4 d). The difference in salinity in the Paratethys basin between the two simulations can also be explained by a different oceanic circulation at the Mediterranean-Paratethys interface. In MioCTL, 0.453 Sv of water flow from the Paratethys to the Mediterranean Sea and 0.452 Sv flow in the opposite direction. In MioTet120, the flows into and out of the Paratethys are reduced to 0.391 Sv and 0.397 Sv respectively (Figure S8). There is therefore more exchange between the Mediterranean Sea and the Paratethys when the eastern Tethys seaway is closed. This is coherent with results from a box-model (Karami, 2011) which infers that the increase in exchange between seas is related to the modulation of flows between Atlantic, Mediterranean, Paratethys and Indian basins but cannot integrate the regional geographic complexity as in our simulations. The flow and exchange variations are certainly due to the different structure of ocean currents in the Mediterranean with an open or close Tethys seaway. The circulation is mainly east-west when the seaway is open, thereby limiting meridional exchanges with the Paratethys. As a concluding aspect, only reliable estimations of the history of the bathymetric evolution of all these seaways (Gibraltar, eastern Tethys, Mediterranean-Paratethys) may improve the understanding of the paleoceanographical dynamics of this region. In general, this shows that the effect of a seaway also depends on the configuration of the other seaways.

4 Conclusion

Our simulations show that in the Early Miocene, NADW was less intense – thus the AMOC was slower – than in the present. This is due to the Miocene palaeogeography (different configurations of some seaways) and may be influenced also by the pCO_2. Greenland glaciation amplifies NADW due to the orographic rise influencing the atmospheric circulation which increases winds and surface currents. This increases the exchange between the North Atlantic and the Arctic, which increases their surface salinities and density. In the Miocene, possible episodes of Greenland glaciation may have favoured and amplified NADW. Hence, the NADW strength in the global ocean circulation today is likely related to the modern Greenland glaciation. On the other hand, the closure of the eastern Tethys seaway does not seem to have a significant impact on the intensity of NADW, conversely to some aspects of modelling studies (Z. Zhang et al., 2011). The closure of the passage causes a significant decrease in water flux from the Mediterranean into the Atlantic Ocean, but without impacting the deep water formation zones.

5 Author Contributions

Q. P. performed the numerical simulations designed by Y. D., and wrote the draft of the manuscript. All authors analyzed and discussed the results and contributed to the final version of the manuscript.

Acknowledgments

We thank the CEA/CCRT for providing access to the HPC resources of TGCC under the allocation 2019-A0050102212 and 2020-A0090102212 made by GENCI and French ANR projects AMOR (YD) and MIOCARD (BSM) for providing funding for this work. Colored figures in this paper were made with perceptually uniform, color-vision-deficiency-friendly scientific color maps, developed and distributed by Fabio Crameri (https://www.fabiocrameri.ch/colourmaps/) (Crameri et al. 2020).

References

Allen, M. B., & Armstrong, H. A. (2008, July). Arabia–Eurasia collision and the forcing of mid-Cenozoic global cooling. *Palaeogeography, Palaeoclimatology, Palaeoecology*, *265*(1-2), 52–58. Retrieved 2021-06-24, from `https://linkinghub.elsevier.com/retrieve/pii/S0031018208002642` doi: 10.1016/j.palaeo.2008.04.021

Aumont, O., Ethé, C., Tagliabue, A., Bopp, L., & Gehlen, M. (2015, August). PISCES-v2: an ocean biogeochemical model for carbon and ecosystem studies. *Geosci. Model Dev.*, *8*(8), 2465–2513. Retrieved 2022-01-03, from `https://gmd.copernicus.org/articles/8/2465/2015/` doi: 10.5194/gmd-8-2465-2015

Bernard, T., Steer, P., Gallagher, K., Szulc, A., Whitham, A., & Johnson, C. (2016, November). Evidence for Eocene–Oligocene glaciation in the landscape of the

East Greenland margin. *Geology*, *44*(11), 895–898. Retrieved 2020-08-28, from https://pubs.geoscienceworld.org/geology/article/44/11/895-898/195070 doi: 10.1130/G38248.1

Bialik, O. M., Frank, M., Betzler, C., Zammit, R., & Waldmann, N. D. (2019, December). Two-step closure of the Miocene Indian Ocean Gateway to the Mediterranean. *Sci Rep*, *9*(1), 8842. Retrieved 2021-06-24, from http://www.nature.com/articles/s41598-019-45308-7 doi: 10.1038/s41598-019-45308-7

Bierman, P. R., Shakun, J. D., Corbett, L. B., Zimmerman, S. R., & Rood, D. H. (2016, December). A persistent and dynamic East Greenland Ice Sheet over the past 7.5 million years. *Nature*, *540*(7632), 256–260. Retrieved from https://doi.org/10.1038/nature20147 doi: 10.1038/nature20147

Borrelli, C., Cramer, B. S., & Katz, M. E. (2014, April). Bipolar Atlantic deepwater circulation in the middle-late Eocene: Effects of Southern Ocean gateway openings. *Paleoceanography*, *29*(4), 308–327. Retrieved 2021-06-11, from http://doi.wiley.com/10.1002/2012PA002444 doi: 10.1002/2012PA002444

Brierley, C. M., & Fedorov, A. V. (2016, June). Comparing the impacts of Miocene–Pliocene changes in inter-ocean gateways on climate: Central American Seaway, Bering Strait, and Indonesia. *Earth and Planetary Science Letters*, *444*, 116–130. Retrieved 2020-08-28, from https://linkinghub.elsevier.com/retrieve/pii/S0012821X16300978 doi: 10.1016/j.epsl.2016.03.010

Burls, N. J., Bradshaw, C., De Boer, A. M., Herold, N., Huber, M., Pound, M., ... Zhang, Z. (2021, January). *Simulating Miocene warmth: insights from an opportunistic Multi-Model ensemble (MioMIP1)* (preprint). Climatology (Global Change). Retrieved 2021-05-06, from http://www.essoar.org/doi/10.1002/essoar.10505870.1 doi: 10.1002/essoar.10505870.1

Burls, N. J., & Fedorov, A. V. (2017, December). Wetter subtropics in a warmer world: Contrasting past and future hydrological cycles. *Proc Natl Acad Sci USA*, *114*(49), 12888–12893. Retrieved 2022-01-11, from http://www.pnas.org/lookup/doi/10.1073/pnas.1703421114 doi: 10.1073/pnas.1703421114

Butt et al., S. S. (2001). Evolution of the Scoresby Sund Fan, central East Greenland evidence from ODP Site 987. , 14.

Capella, W., Flecker, R., Hernández-Molina, F. J., Simon, D., Meijer, P. T., Rogerson, M., ... Krijgsman, W. (2019, December). Mediterranean isolation preconditioning the Earth System for late Miocene climate cooling. *Sci Rep*, *9*(1), 3795. Retrieved 2021-01-05, from http://www.nature.com/articles/s41598-019-40208-2 doi: 10.1038/s41598-019-40208-2

Coxall, H. K., Huck, C. E., Huber, M., Lear, C. H., Legarda-Lisarri, A., O'Regan, M., ... Backman, J. (2018, March). Export of nutrient rich Northern Component Water preceded earlyOligocene Antarctic glaciation. *Nature Geosci*, *11*(3), 190–196. Retrieved 2021-06-11, from http://www.nature.com/articles/s41561-018-0069-9 doi: 10.1038/s41561-018-0069-9

Davies, R., Cartwright, J., Pike, J., & Line, C. (2001, April). Early Oligocene initiation of North Atlantic Deep Water formation. *Nature*, *410*(6831), 917–920. Retrieved 2021-06-11, from http://www.nature.com/articles/35073551 doi: 10.1038/35073551

Davini, P., von Hardenberg, J., Filippi, L., & Provenzale, A. (2015, February). Impact of Greenland orography on the Atlantic Meridional Overturning Circulation. *Geophys. Res. Lett.*, *42*(3), 871–879. Retrieved 2020-08-28, from http://doi.wiley.com/10.1002/2014GL062668 doi: 10.1002/2014GL062668

DeConto, R. M., Pollard, D., Wilson, P. A., Pälike, H., Lear, C. H., & Pagani,

M. (2008, October). Thresholds for Cenozoic bipolar glaciation. *Nature*, *455*(7213), 652–656. Retrieved 2021-08-17, from http://www.nature.com/articles/nature07337 doi: 10.1038/nature07337

de la Vara, A., & Meijer, P. (2016, January). Response of Mediterranean circulation to Miocene shoaling and closure of the Indian Gateway: A model study. *Palaeogeography, Palaeoclimatology, Palaeoecology*, *442*, 96–109. Retrieved 2020-08-28, from https://linkinghub.elsevier.com/retrieve/pii/S0031018215006252 doi: 10.1016/j.palaeo.2015.11.002

Dufresne, J.-L., Foujols, M.-A., Denvil, S., Caubel, A., Marti, O., Aumont, O., ... Vuichard, N. (2013, May). Climate change projections using the IPSL-CM5 Earth System Model: from CMIP3 to CMIP5. *Clim Dyn*, *40*(9-10), 2123–2165. Retrieved 2022-01-03, from http://link.springer.com/10.1007/s00382-012-1636-1 doi: 10.1007/s00382-012-1636-1

Eldrett, J. S., Harding, I. C., Wilson, P. A., Butler, E., & Roberts, A. P. (2007, March). Continental ice in Greenland during the Eocene and Oligocene. *Nature*, *446*(7132), 176–179. Retrieved 2021-06-24, from http://www.nature.com/articles/nature05591 doi: 10.1038/nature05591

Ferreira, D., Cessi, P., Coxall, H. K., de Boer, A., Dijkstra, H. A., Drijfhout, S. S., ... Wills, R. C. (2018, May). Atlantic-Pacific Asymmetry in Deep Water Formation. *Annu. Rev. Earth Planet. Sci.*, *46*(1), 327–352. Retrieved 2021-06-21, from https://www.annualreviews.org/doi/10.1146/annurev-earth-082517-010045 doi: 10.1146/annurev-earth-082517-010045

Fichefet, T., & Maqueda, M. A. M. (1997, June). Sensitivity of a global sea ice model to the treatment of ice thermodynamics and dynamics. *J. Geophys. Res.*, *102*(C6), 12609–12646. Retrieved 2022-01-03, from http://doi.wiley.com/10.1029/97JC00480 doi: 10.1029/97JC00480

Flecker, R., Krijgsman, W., Capella, W., de Castro Martíns, C., Dmitrieva, E., Mayser, J. P., ... Yousfi, M. Z. (2015, November). Evolution of the Late Miocene Mediterranean–Atlantic gateways and their impact on regional and global environmental change. *Earth-Science Reviews*, *150*, 365–392. Retrieved 2021-12-29, from https://linkinghub.elsevier.com/retrieve/pii/S0012825215300313 doi: 10.1016/j.earscirev.2015.08.007

Hamon, N., Sepulchre, P., Lefebvre, V., & Ramstein, G. (2013, November). The role of eastern Tethys seaway closure in the Middle Miocene Climatic Transition (ca. 14 Ma). *Clim. Past*, *9*(6), 2687–2702. Retrieved 2020-08-28, from https://cp.copernicus.org/articles/9/2687/2013/ doi: 10.5194/cp-9-2687-2013

Harzhauser, M., Kroh, A., Mandic, O., Piller, W. E., Göhlich, U., Reuter, M., & Berning, B. (2007, December). Biogeographic responses to geodynamics: A key study all around the Oligo–Miocene Tethyan Seaway. *Zoologischer Anzeiger - A Journal of Comparative Zoology*, *246*(4), 241–256. Retrieved 2021-06-24, from https://linkinghub.elsevier.com/retrieve/pii/S0044523107000186 doi: 10.1016/j.jcz.2007.05.001

Harzhauser, M., Reuter, M., Piller, W. E., Berning, B., Kroh, A., & Mandic, O. (2009, September). Oligocene and Early Miocene gastropods from Kutch (NW India) document an early biogeographic switch from Western Tethys to Indo-Pacific. *Paläontol. Z.*, *83*(3), 333–372. Retrieved 2021-06-24, from http://link.springer.com/10.1007/s12542-009-0025-5 doi: 10.1007/s12542-009-0025-5

Helland, P., & Holmes, M. (1997, December). Surface textural analysis of quartz sand grains from ODP Site 918 off the southeast coast of Greenland suggests glaciation of southern Greenland at 11 Ma. *Palaeogeography, Palaeoclimatology, Palaeoecology*, *135*(1-4), 109–121. Retrieved 2021-08-17, from https://linkinghub.elsevier.com/retrieve/pii/S0031018297000254 doi: 10.1016/S0031-0182(97)00025-4

Herold, N., Huber, M., & Müller, R. D. (2011, December). Modeling the Miocene Climatic Optimum. Part I: Land and Atmosphere*. *Journal of Climate*, *24*(24), 6353–6372. Retrieved 2021-08-31, from http://journals.ametsoc.org/doi/10.1175/2011JCLI4035.1 doi: 10.1175/2011JCLI4035.1

Hossain, A., Knorr, G., Lohmann, G., Stärz, M., & Jokat, W. (2020, July). Simulated Thermohaline Fingerprints in Response to Different Greenland-Scotland Ridge and Fram Strait Subsidence Histories. *Paleoceanography and Paleoclimatology*, *35*(7). Retrieved 2021-05-10, from https://onlinelibrary.wiley.com/doi/abs/10.1029/2019PA003842 doi: 10.1029/2019PA003842

Hourdin, F., Foujols, M.-A., Codron, F., Guemas, V., Dufresne, J.-L., Bony, S., ... Bopp, L. (2013, May). Impact of the LMDZ atmospheric grid configuration on the climate and sensitivity of the IPSL-CM5A coupled model. *Clim Dyn*, *40*(9-10), 2167–2192. Retrieved 2022-01-03, from http://link.springer.com/10.1007/s00382-012-1411-3 doi: 10.1007/s00382-012-1411-3

Hu, A., Meehl, G. A., Han, W., Otto-Bliestner, B., Abe-Ouchi, A., & Rosenbloom, N. (2015, March). Effects of the Bering Strait closure on AMOC and global climate under different background climates. *Progress in Oceanography*, *132*, 174–196. Retrieved 2022-01-03, from https://linkinghub.elsevier.com/retrieve/pii/S0079661114000172 doi: 10.1016/j.pocean.2014.02.004

Hüsing, S. K., Zachariasse, W.-J., van Hinsbergen, D. J. J., Krijgsman, W., Inceöz, M., Harzhauser, M., ... Kroh, A. (2009). Oligocene–Miocene basin evolution in SE Anatolia, Turkey: constraints on the closure of the eastern Tethys gateway. *Geological Society, London, Special Publications*, *311*(1), 107–132. Retrieved 2021-06-24, from http://sp.lyellcollection.org/lookup/doi/10.1144/SP311.4 doi: 10.1144/SP311.4

Ivanovic, R. F., Valdes, P. J., Flecker, R., Gregoire, L. J., & Gutjahr, M. (2013, February). The parameterisation of Mediterranean–Atlantic water exchange in the Hadley Centre model HadCM3, and its effect on modelled North Atlantic climate. *Ocean Modelling*, *62*, 11–16. Retrieved 2021-12-29, from https://linkinghub.elsevier.com/retrieve/pii/S146350031200162X doi: 10.1016/j.ocemod.2012.11.002

Jakobsson, M., Backman, J., Rudels, B., Nycander, J., Frank, M., Mayer, L., ... Moran, K. (2007, June). The early Miocene onset of a ventilated circulation regime in the Arctic Ocean. *Nature*, *447*(7147), 986–990. Retrieved 2021-06-11, from http://www.nature.com/articles/nature05924 doi: 10.1038/nature05924

John, S., & Krissek, L. A. (2002). The late Miocene to Pleistocene ice-rafting history of southeast Greenland. , 8.

Karami, M. P. (2011). The role of gateways in the evolution of temperature and salinity of semi-enclosed basins: An oceanic box model for the Miocene Mediterranean Sea and Paratethys. *Global and Planetary Change*, 17.

Katz, M. E., Cramer, B. S., Toggweiler, J. R., Esmay, G., Liu, C., Miller, K. G., ... Wright, J. D. (2011, May). Impact of Antarctic Circumpolar Current Development on Late Paleogene Ocean Structure. *Science*, *332*(6033), 1076–1079. Retrieved 2021-07-05, from https://www.sciencemag.org/lookup/doi/10.1126/science.1202122 doi: 10.1126/science.1202122

Knutz, P. C., Hopper, J. R., Gregersen, U., Nielsen, T., & Japsen, P. (2015, October). A contourite drift system on the Baffin Bay–West Greenland margin linking Pliocene Arctic warming to poleward ocean circulation. *Geology*, *43*(10), 907–910. Retrieved 2021-06-24, from https://pubs.geoscienceworld.org/geology/article/43/10/907-910/131734 doi: 10.1130/G36927.1

Krapp, M., & Jungclaus, J. H. (2011, November). The Middle Miocene climate as modelled in an atmosphere-ocean-biosphere model. *Clim. Past*, *7*(4), 1169–1188. Retrieved 2021-05-10, from https://cp.copernicus.org/articles/7/1169/2011/ doi: 10.5194/cp-7-1169-2011

Krinner, G., Viovy, N., de Noblet-Ducoudré, N., Ogée, J., Polcher, J., Friedlingstein, P., ... Prentice, I. C. (2005, March). A dynamic global vegetation model for studies of the coupled atmosphere-biosphere system: DVGM FOR COUPLED CLIMATE STUDIES. *Global Biogeochem. Cycles*, *19*(1). Retrieved 2022-01-03, from http://doi.wiley.com/10.1029/2003GB002199 doi: 10.1029/2003GB002199

Langton, S. J., Rabideaux, N. M., Borrelli, C., & Katz, M. E. (2016, June). Southeastern Atlantic deep-water evolution during the late-middle Eocene to earliest Oligocene (Ocean Drilling Program Site 1263 and Deep Sea Drilling Project Site 366). *Geosphere*, *12*(3), 1032–1047. Retrieved 2021-06-11, from https://pubs.geoscienceworld.org/geosphere/article/12/3/1032-1047/132329 doi: 10.1130/GES01268.1

Lunt, D. J., de Noblet-Ducoudré, N., & Charbit, S. (2004, December). Effects of a melted greenland ice sheet on climate, vegetation, and the cryosphere. *Climate Dynamics*, *23*(7-8), 679–694. Retrieved 2020-08-28, from http://link.springer.com/10.1007/s00382-004-0463-4 doi: 10.1007/s00382-004-0463-4

Madec, G. (2015). NEMO ocean engine. , 396.

Maffre, P., Ladant, J.-B., Donnadieu, Y., Sepulchre, P., & Goddéris, Y. (2018, February). The influence of orography on modern ocean circulation. *Clim Dyn*, *50*(3-4), 1277–1289. Retrieved 2020-08-28, from http://link.springer.com/10.1007/s00382-017-3683-0 doi: 10.1007/s00382-017-3683-0

Ng, Z. L., Hernández-Molina, F. J., Duarte, D., Sierro, F. J., Ledesma, S., Rogerson, M., ... Manar, M. A. (2021, June). Latest Miocene restriction of the Mediterranean Outflow Water: a perspective from the Gulf of Cádiz. *Geo-Mar Lett*, *41*(2), 23. Retrieved 2021-12-29, from https://link.springer.com/10.1007/s00367-021-00693-9 doi: 10.1007/s00367-021-00693-9

Nisancioglu, K. H., Raymo, M. E., & Stone, P. H. (2003, March). Reorganization of Miocene deep water circulation in response to the shoaling of the Central American Seaway: REORGANIZATION OF MIOCENE DEEP WATER CIRCULATION. *Paleoceanography*, *18*(1), n/a–n/a. Retrieved 2021-05-10, from http://doi.wiley.com/10.1029/2002PA000767 doi: 10.1029/2002PA000767

Okay, A. I., Zattin, M., & Cavazza, W. (2010, January). Apatite fission-track data for the Miocene Arabia-Eurasia collision. *Geology*, *38*(1), 35–38. Retrieved 2021-06-24, from http://pubs.geoscienceworld.org/geology/article/38/1/35/130073/Apatite-fissiontrack-data-for-the-Miocene doi: 10.1130/G30234.1

Poblete, F., Dupont-Nivet, G., Licht, A., van Hinsbergen, D., Roperch, P., Mihalynuk, M., ... Baatsen, M. (2021, March). Towards interactive global paleogeographic maps, new reconstructions at 60, 40 and 20 Ma. *Earth-Science Reviews*, *214*, 103508. Retrieved 2021-07-01, from https://linkinghub.elsevier.com/retrieve/pii/S0012825221000076 doi: 10.1016/j.earscirev.2021.103508

Poore, H. R., Samworth, R., White, N. J., Jones, S. M., & McCave, I. N. (2006, June). Neogene overflow of Northern Component Water at the Greenland-Scotland Ridge: NEOGENE OVERFLOW OF NCW. *Geochem. Geophys. Geosyst.*, *7*(6), n/a–n/a. Retrieved 2020-08-28, from http://doi.wiley.com/10.1029/2005GC001085 doi: 10.1029/2005GC001085

Rae, J. W., Zhang, Y. G., Liu, X., Foster, G. L., Stoll, H. M., & Whiteford, R. D. (2021, May). Atmospheric CO $_2$ over the Past 66 Million Years from Marine Archives. *Annu. Rev. Earth Planet. Sci.*, *49*(1), 609–641. Retrieved 2021-09-01, from https://www.annualreviews.org/doi/10.1146/annurev-earth-082420-063026 doi: 10.1146/annurev-earth-082420-063026

Reuter, M., Piller, W. E., Harzhauser, M., Mandic, O., Berning, B., Rögl, F., ...

Hamedani, A. (2009, April). The Oligo-/Miocene Qom Formation (Iran): evidence for an early Burdigalian restriction of the Tethyan Seaway and closure of its Iranian gateways. *Int J Earth Sci (Geol Rundsch)*, *98*(3), 627–650. Retrieved 2021-06-24, from `http://link.springer.com/10.1007/s00531-007-0269-9` doi: 10.1007/s00531-007-0269-9

Rögl, F. (1999). MEDITERRANEAN AND PARATETHYS. FACTS AND HYPOTHESES OF AN OLIGOCENE TO MIOCENE PALEOGEOGRAPHY (SHORT OVERVIEW). , 11.

Scher, H. D., & Martin, E. E. (2008, March). Oligocene deep water export from the North Atlantic and the development of the Antarctic Circumpolar Current examined with neodymium isotopes: OLIGOCENE THERMOHALINE TRANSITION. *Paleoceanography*, *23*(1), n/a–n/a. Retrieved 2021-06-11, from `http://doi.wiley.com/10.1029/2006PA001400` doi: 10.1029/2006PA001400

Schneider, B., & Schmittner, A. (2006, June). Simulating the impact of the Panamanian seaway closure on ocean circulation, marine productivity and nutrient cycling. *Earth and Planetary Science Letters*, *246*(3-4), 367–380. Retrieved 2021-10-28, from `https://linkinghub.elsevier.com/retrieve/pii/S0012821X0600330X` doi: 10.1016/j.epsl.2006.04.028

Sepulchre, P., Arsouze, T., Donnadieu, Y., Dutay, J.-C., Jaramillo, C., Le Bras, J., ... Waite, A. J. (2014, March). Consequences of shoaling of the Central American Seaway determined from modeling Nd isotopes. *Paleoceanography*, *29*(3), 176–189. Retrieved 2021-05-10, from `http://doi.wiley.com/10.1002/2013PA002501` doi: 10.1002/2013PA002501

Sepulchre, P., Caubel, A., Ladant, J.-B., Bopp, L., Boucher, O., Braconnot, P., ... Tardif, D. (2020, July). IPSL-CM5A2 – an Earth system model designed for multi-millennial climate simulations. *Geosci. Model Dev.*, *13*(7), 3011–3053. Retrieved 2022-01-03, from `https://gmd.copernicus.org/articles/13/3011/2020/` doi: 10.5194/gmd-13-3011-2020

Sosdian, S. M., Greenop, R., Hain, M. P., Foster, G. L., Pearson, P. N., & Lear, C. H. (2018, September). Constraining the evolution of Neogene ocean carbonate chemistry using the boron isotope pH proxy. *Earth and Planetary Science Letters*, *498*, 362–376. Retrieved 2021-09-01, from `https://www.sciencedirect.com/science/article/pii/S0012821X1830356X` doi: 10.1016/j.epsl.2018.06.017

Stärz, M., Jokat, W., Knorr, G., & Lohmann, G. (2017, August). Threshold in North Atlantic-Arctic Ocean circulation controlled by the subsidence of the Greenland-Scotland Ridge. *Nat Commun*, *8*(1), 15681. Retrieved 2021-05-10, from `http://www.nature.com/articles/ncomms15681` doi: 10.1038/ncomms15681

Sun, J., Sheykh, M., Ahmadi, N., Cao, M., Zhang, Z., Tian, S., ... Talebian, M. (2021, February). Permanent closure of the Tethyan Seaway in the northwestern Iranian Plateau driven by cyclic sea-level fluctuations in the late Middle Miocene. *Palaeogeography, Palaeoclimatology, Palaeoecology*, *564*, 110172. Retrieved 2021-06-15, from `https://linkinghub.elsevier.com/retrieve/pii/S0031018220306209` doi: 10.1016/j.palaeo.2020.110172

Talley, L. (2013, March). Closure of the Global Overturning Circulation Through the Indian, Pacific, and Southern Oceans: Schematics and Transports. *oceanog*, *26*(1), 80–97. Retrieved 2020-08-28, from `https://tos.org/oceanography/article/closure-of-the-global-overturning-circulation-through-the-indian-pacific-an` doi: 10.5670/oceanog.2013.07

Toniazzo, T., Gregory, J. M., & Huybrechts, P. (2004). Climatic Impact of a Greenland Deglaciation and Its Possible Irreversibility. *JOURNAL OF CLIMATE*, *17*, 13.

Tripati, A. K., Eagle, R. A., Morton, A., Dowdeswell, J. A., Atkinson, K. L., Bahé, Y., ... Thanabalasundaram, L. (2008, January). Evidence for glaciation in the Northern Hemisphere back to 44 Ma from ice-rafted debris in the Greenland Sea. *Earth and Planetary Science Letters*, *265*(1-2), 112–122. Retrieved 2021-06-24, from https://linkinghub.elsevier.com/retrieve/pii/S0012821X07006103 doi: 10.1016/j.epsl.2007.09.045

Valcke, S. (2013, March). The OASIS3 coupler: a European climate modelling community software. *Geosci. Model Dev.*, *6*(2), 373–388. Retrieved 2022-01-03, from https://gmd.copernicus.org/articles/6/373/2013/ doi: 10.5194/gmd-6-373-2013

Via, R. K., & Thomas, D. J. (2006). Evolution of Atlantic thermohaline circulation: Early Oligocene onset of deep-water production in the North Atlantic. *Geol*, *34*(6), 441. Retrieved 2021-06-11, from https://pubs.geoscienceworld.org/geology/article/34/6/441-444/129556 doi: 10.1130/G22545.1

von der Heydt, A., & Dijkstra, H. A. (2006, March). Effect of ocean gateways on the global ocean circulation in the late Oligocene and early Miocene: OLIGOCENE/MIOCENE OCEAN CIRCULATION. *Paleoceanography*, *21*(1), n/a–n/a. Retrieved 2020-08-28, from http://doi.wiley.com/10.1029/2005PA001149 doi: 10.1029/2005PA001149

Woodruff, F., & Savin, S. M. (1989, February). Miocene deepwater oceanography. *Paleoceanography*, *4*(1), 87–140. Retrieved 2021-06-11, from http://doi.wiley.com/10.1029/PA004i001p00087 doi: 10.1029/PA004i001p00087

Wright, J. D., & Miller, K. G. (1993). Southern Ocean influences on late Eocene to Miocene deepwater circulation. In J. P. Kennett & D. A. Warnke (Eds.), *Antarctic Research Series* (Vol. 60, pp. 1–25). Washington, D. C.: American Geophysical Union. Retrieved 2021-06-11, from http://www.agu.org/books/ar/v060/AR060p0001/AR060p0001.shtml doi: 10.1029/AR060p0001

Wright, J. D., Miller, K. G., & Fairbanks, R. G. (1992). Early and Middle Miocene stable isotopes: Implications for Deepwater circulation and climate. *Paleoceanography*, *7*(3), 357–389. Retrieved 2021-12-22, from http://onlinelibrary.wiley.com/doi/abs/10.1029/92PA00760 (_eprint: https://agupubs.onlinelibrary.wiley.com/doi/pdf/10.1029/92PA00760) doi: 10.1029/92PA00760

Zhang, Y., Huck, T., Lique, C., Donnadieu, Y., Ladant, J.-B., Rabineau, M., & Aslanian, D. (2020, July). Early Eocene vigorous ocean overturning and its contribution to a warm Southern Ocean. *Clim. Past*, *16*(4), 1263–1283. Retrieved 2022-01-11, from https://cp.copernicus.org/articles/16/1263/2020/ doi: 10.5194/cp-16-1263-2020

Zhang, Z., Nisancioglu, K. H., Flatøy, F., Bentsen, M., Bethke, I., & Wang, H. (2011, July). Tropical seaways played a more important role than high latitude seaways in Cenozoic cooling. *Clim. Past*, *7*(3), 801–813. Retrieved 2020-08-28, from https://cp.copernicus.org/articles/7/801/2011/ doi: 10.5194/cp-7-801-2011

Figure 1.

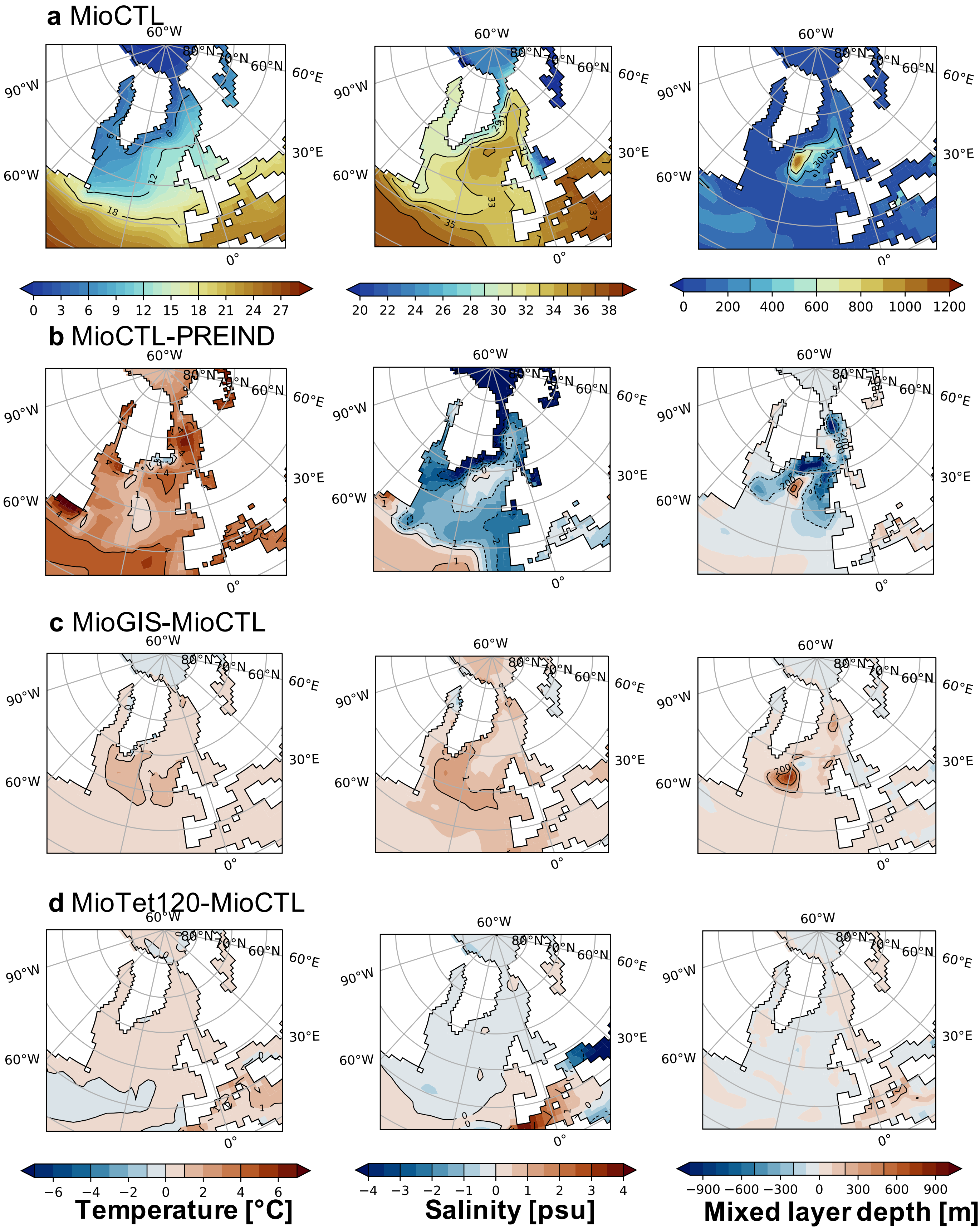

a MioCTL
b MioCTL-PREIND
c MioGIS-MioCTL
d MioTet120-MioCTL
60°W
80°N
70°N
60°N
60°E
90°W
30°E
0°
0 3 6 9 12 15 18 21 24 27
20 22 24 26 28 30 32 34 36 38
0 200 400 600 800 1000 1200
−6 −4 −2 0 2 4 6
−4 −3 −2 −1 0 1 2 3 4
−900 −600 −300 0 300 600 900
Temperature [°C]
Salinity [psu]
Mixed layer depth [m]

Figure 2.

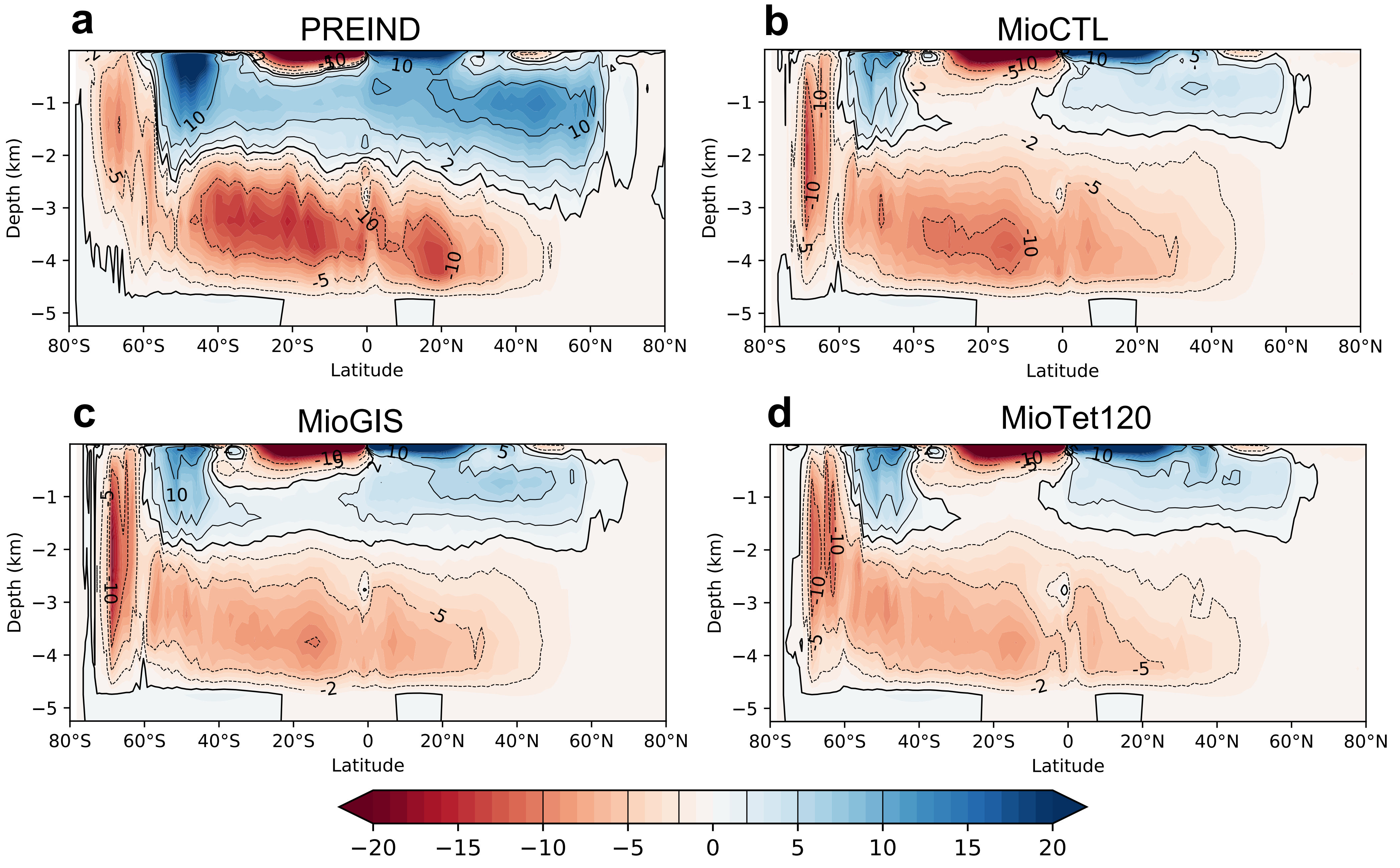

a
PREIND
b
MioCTL
c
MioGIS
d
MioTet120
Depth (km)
Latitude
80°S 60°S 40°S 20°S 0 20°N 40°N 60°N 80°N
−20 −15 −10 −5 0 5 10 15 20

Figure 3.

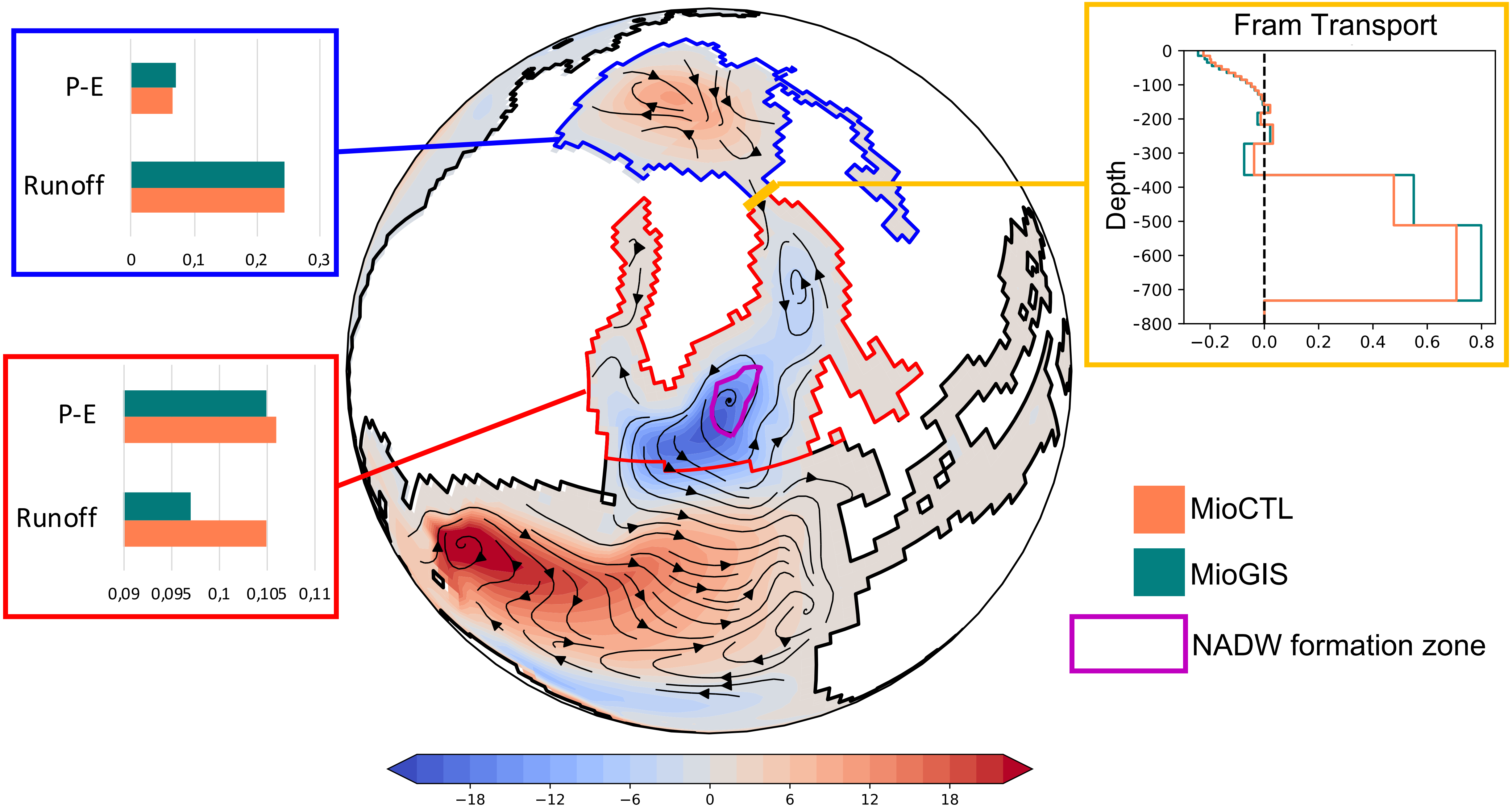
P-E
Runoff
0
0,1
0,2
0,3
P-E
Runoff
0,09
0,095
0,1
0,105
0,11
Fram Transport
Depth
0
-100
-200
-300
-400
-500
-600
-700
-800
−0.2
0.0
0.2
0.4
0.6
0.8
MioCTL
MioGIS
NADW formation zone
−18
−12
−6
0
6
12
18

Figure 4.

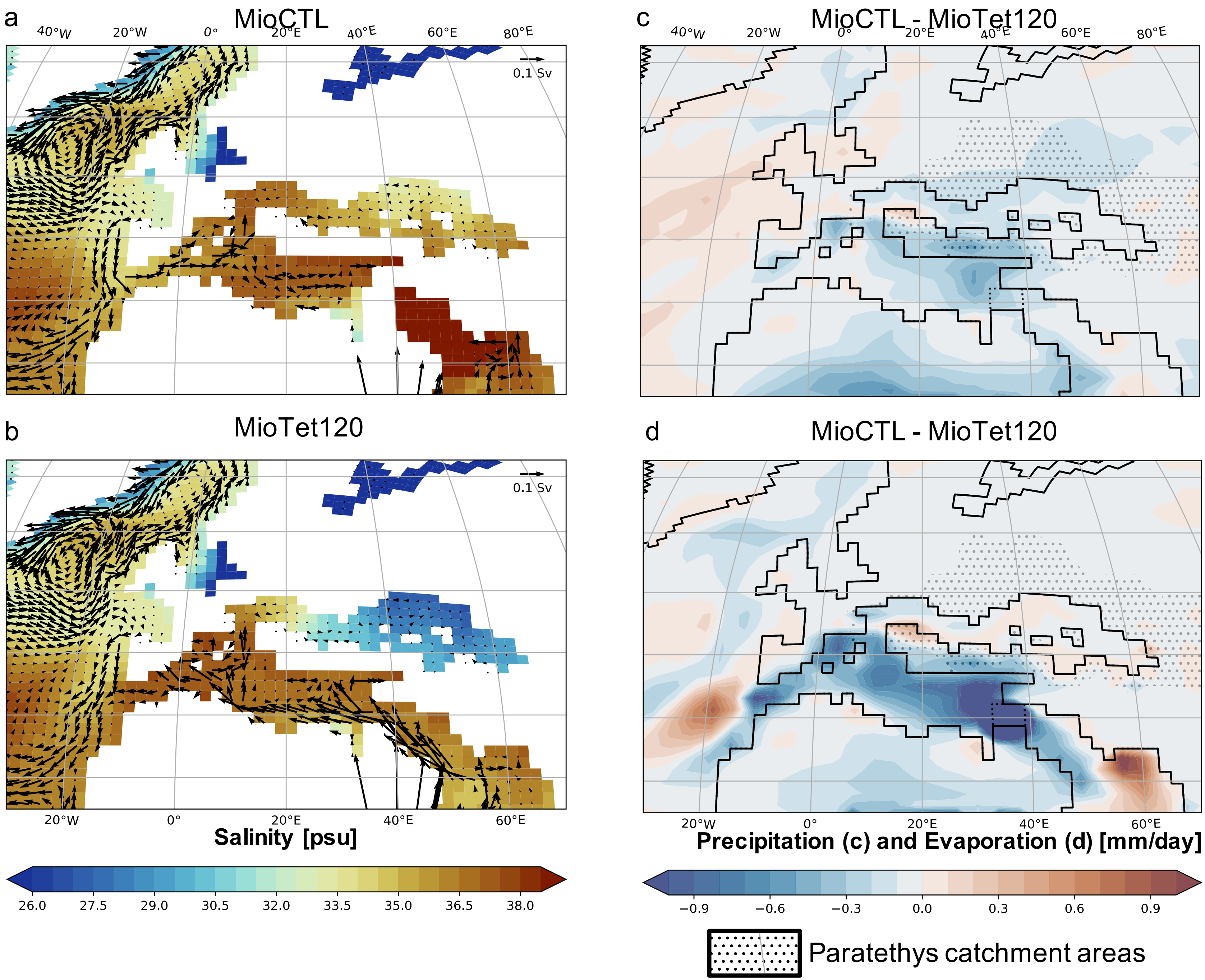

a
MioCTL
b
MioTet120
c
MioCTL - MioTet120
d
MioCTL - MioTet120
0.1 Sv
Salinity [psu]
26.0
27.5
29.0
30.5
32.0
33.5
35.0
36.5
38.0
Precipitation (c) and Evaporation (d) [mm/day]
−0.9
−0.6
−0.3
0.0
0.3
0.6
0.9
Paratethys catchment areas

Supporting Information for "Evolution of ocean circulation in the North Atlantic Ocean during the Miocene : impact of the Greenland ice sheet and the eastern Tethys seaway"

Pillot Q.[1], Donnadieu Y.[1], Sarr A-C.[1], Ladant J-B.[2]and Suchéras-Marx B.[1]

[1]CEREGE, Aix Marseille Univ, CNRS, IRD, INRAE, Coll. France, France.

[2]Laboratoire des Sciences du Climat et de l'Environnement, LSCE/IPSL, CEA-CNRS-UVSQ, Université Paris-Saclay, France.

Contents of this file

Figures S1 to S8

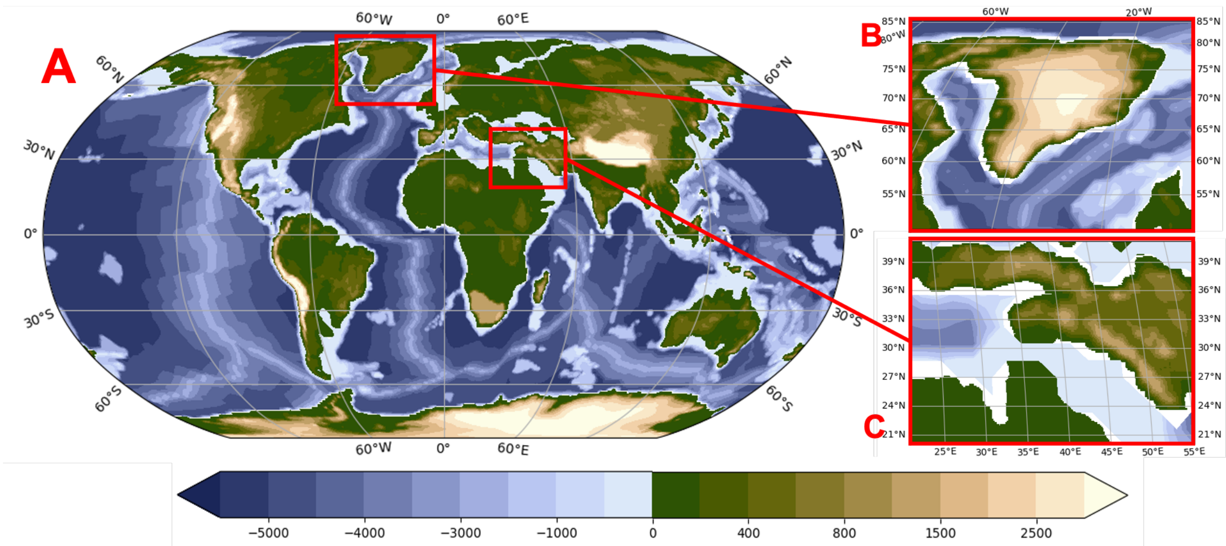

Figure S1. Topography and bathymetry of the simulations (in meters). (A) MioCTL, (B) MioGIS and (C) MioTet120.

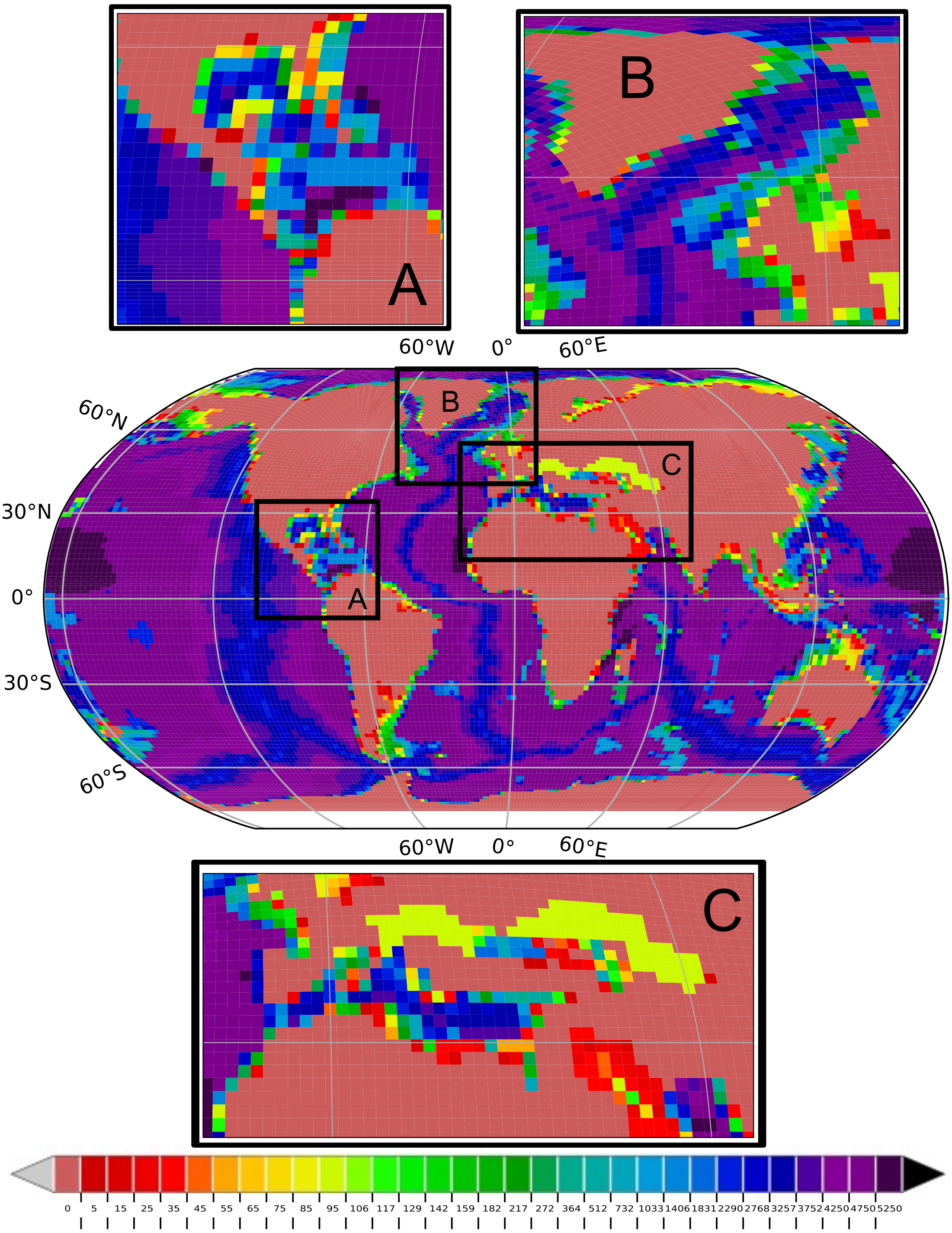

Figure S2. Bathymetry of the simulation MioCTL (in meters) for the 31 levels of the model.

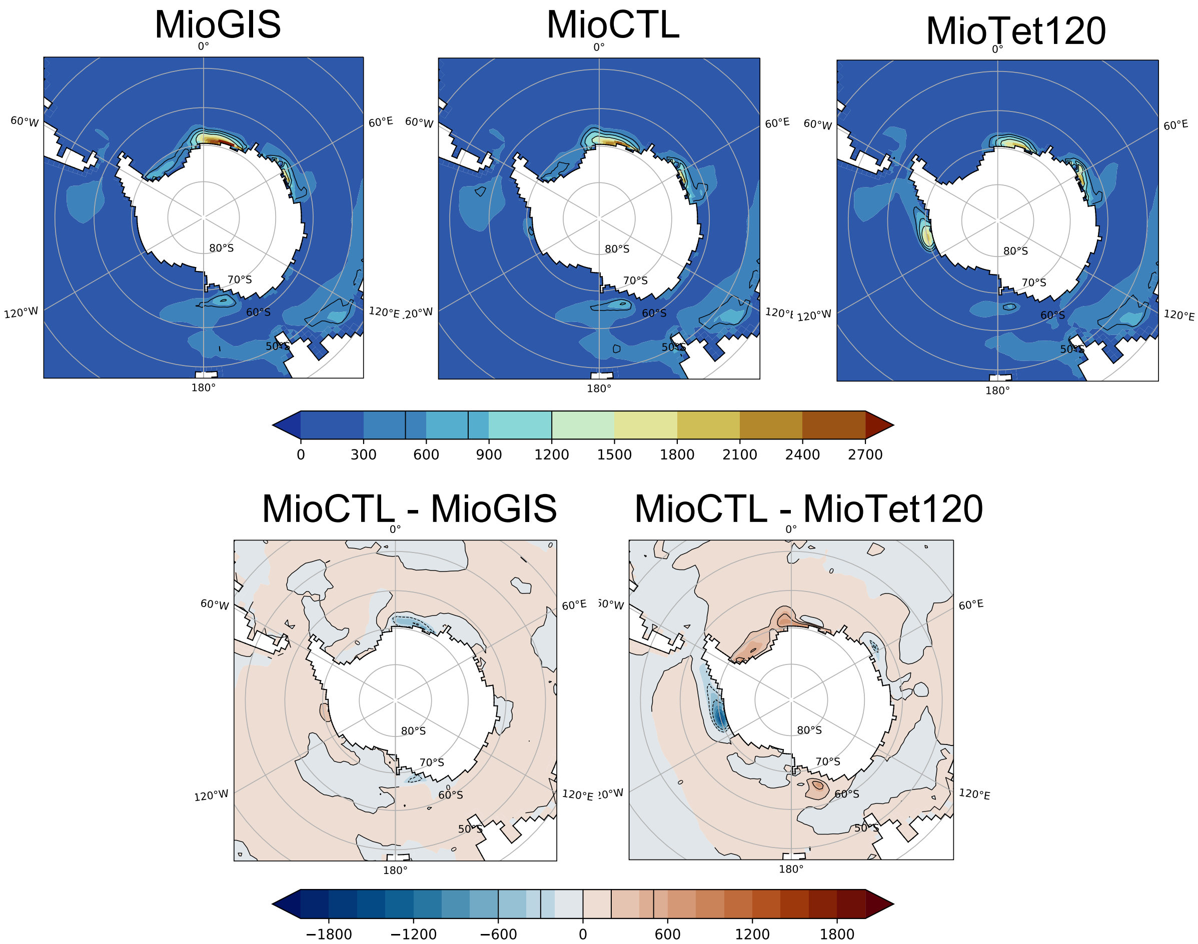

Figure S3. Depth of the mixing layer in meters, averaged over the southern winter, in the southern ocean for MioGIS ,MioCTL, MioTet120 and the differences MioCTL-MioGIS and MioCTL-MioTet120.

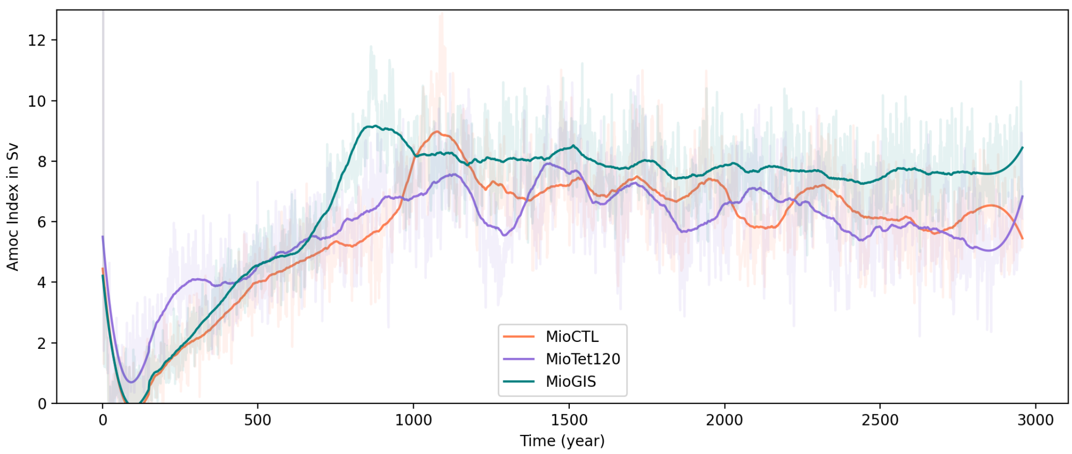

Figure S4. Temporal evolution of the AMOC index in Sv (yearly maximum of the meridional stream function between 38°N and 50°N and between 500 and 2000 m depth) on the 3000 years of simulations (average over 300 year).

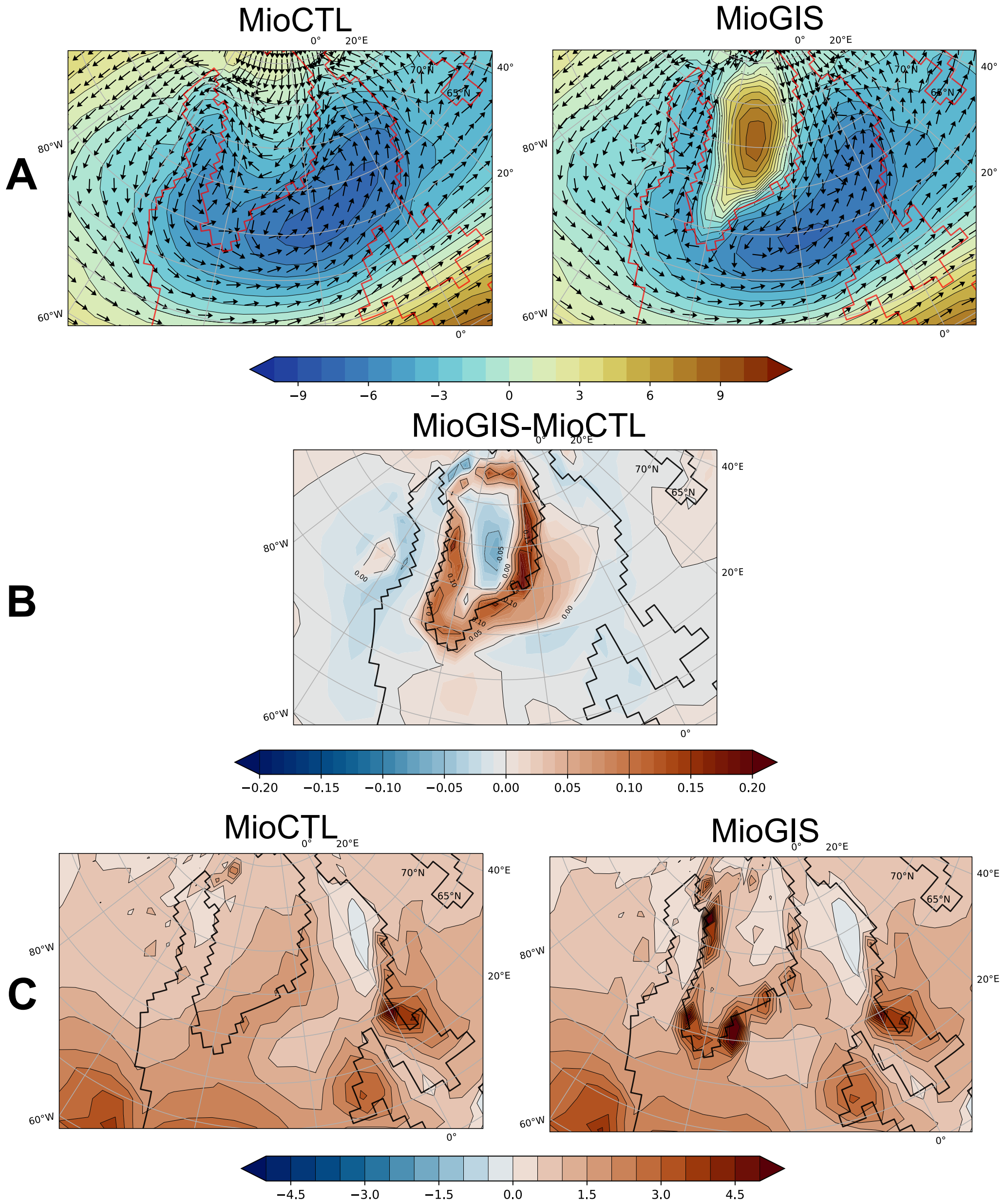

Figure S5. (A) In color, pressure anomaly (hPa), averaged over the winter, at ground level. The arrows indicate the average wind direction at 850 hPa. (B) Difference in wind stress averaged over the year MioGIS-MioCTL. (C) Precipitation - evaporation (mm/day), averaged over the year.

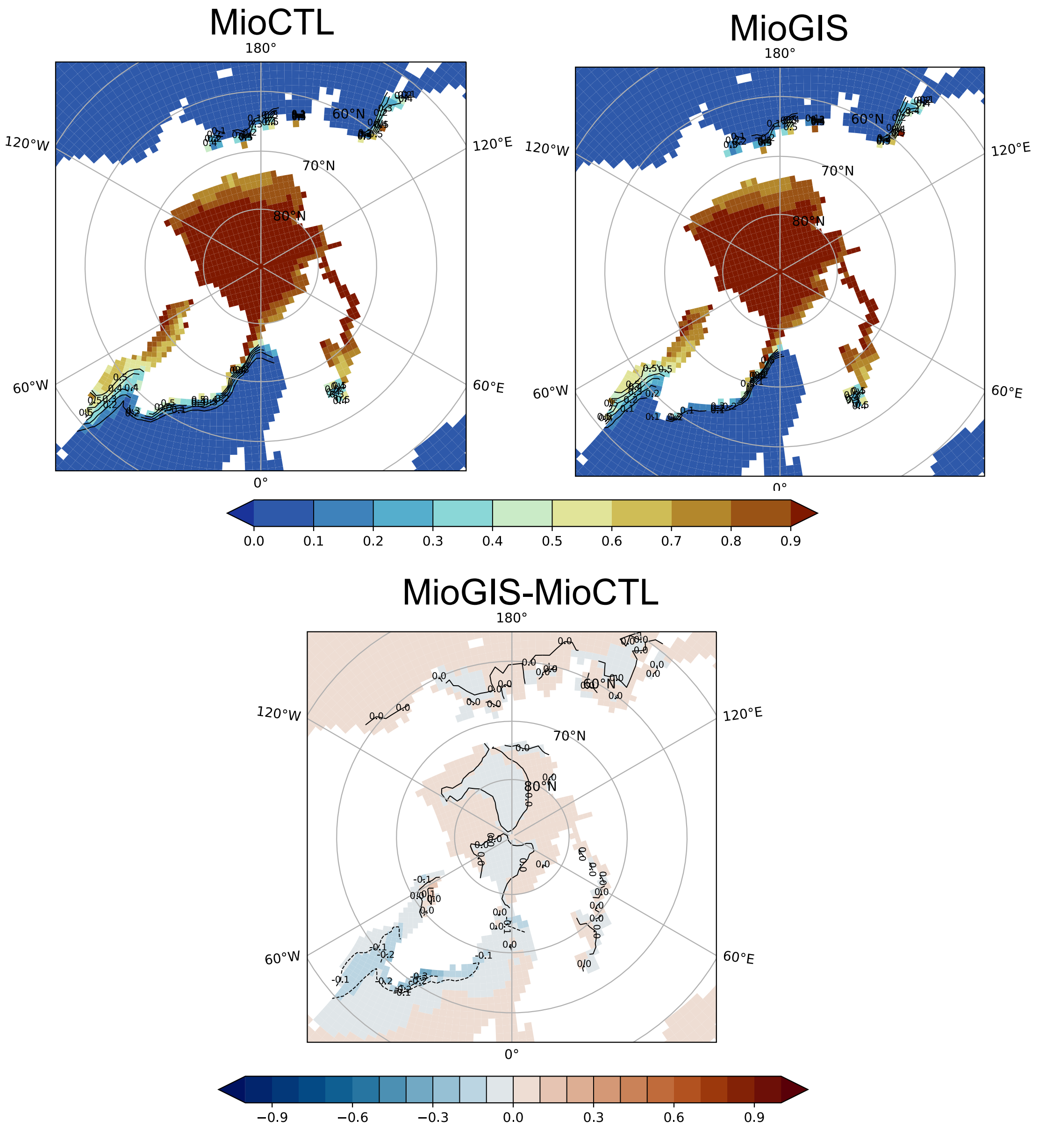

Figure S6. Sea ice concentration (%), averaged over the winter for MioCTL,MioGIS and the differences MioGIS-MioCTL.

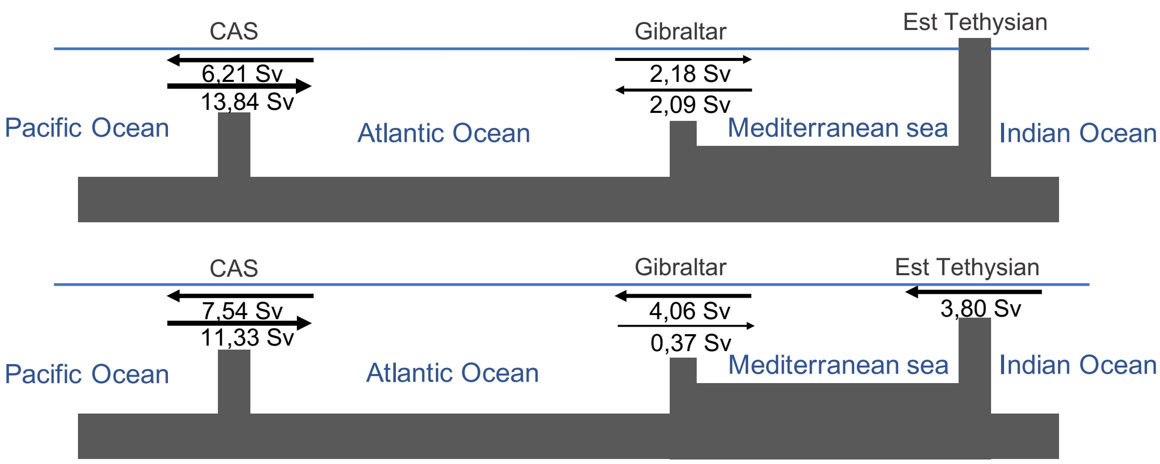

Figure S7. Diagram of the flow exchanges (Sv) through the CAS seaway, the Strait of Gibraltar and the eastern Tethys seaway. At the top, the MioCTL simulation and at the bottom, the MioTet120 simulation.

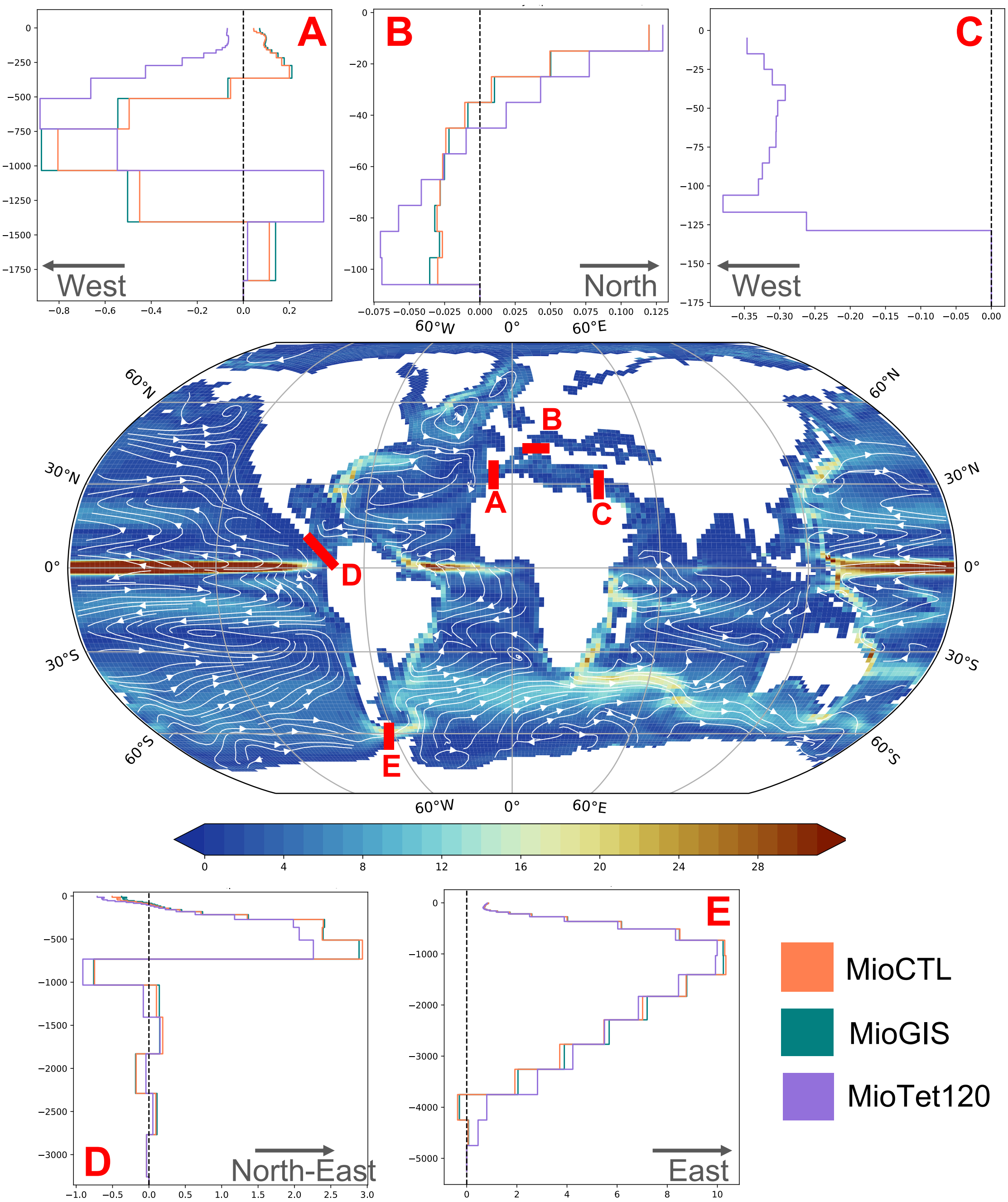

Figure S8. Water mass transport in Sv through different seaways with depth (A: Gibraltar, B: Paratethys, C: East-Tethys, D: Panama, E: Drake). A,C,E : positive eastwards and negative westwards, B : positive northwards and negative southwards, D : positive eastwards/northwards and negative westwards/southwards. Map: water mass transport in Sv, averaged over the first 100 metres and over the year for the MioCTL simulation.